

HST/ACS OBSERVATIONS OF RR LYRAE STARS IN SIX ULTRA-DEEP FIELDS OF M31¹

ELIZABETH J. JEFFERY², ED SMITH², THOMAS M. BROWN², ALLEN V. SWEIGART³, JASON KALIRAI², HENRY C. FERGUSON²,
PURAGRA GUHATHAKURTA⁴, ALVIO RENZINI⁵, R. MICHAEL RICH⁶

Draft version November 1, 2018

ABSTRACT

We present HST/ACS observations of RR Lyrae variable stars in six ultra deep fields of the Andromeda galaxy (M31), including parts of the halo, disk, and giant stellar stream. Past work on the RR Lyrae stars in M31 has focused on various aspects of the stellar populations that make up the galaxy's halo, including their distances and metallicities. This study builds upon this previous work by increasing the spatial coverage (something that has been lacking in previous studies) and by searching for these variable stars in constituents of the galaxy not yet explored. Besides the 55 RR Lyrae stars we found in our initial field located 11kpc from the galactic nucleus, we find additional RR Lyrae stars in four of the remaining five ultra deep fields as follows: 21 in the disk, 24 in the giant stellar stream, 3 in the halo field 21kpc from the galactic nucleus, and 5 in one of the halo fields at 35kpc. No RR Lyrae were found in the second halo field at 35kpc. The RR Lyrae populations of these fields appear to mostly be of Oosterhoff I type, although the 11kpc field appears to be intermediate or mixed. We will discuss the properties of these stars including period and reddening distributions. We calculate metallicities and distances for the stars in each of these fields using different methods and compare the results, to an extent that has not yet been done. We compare these methods not just on RR Lyrae stars in our M31 fields, but also on a data set of Milky Way field RR Lyrae stars.

Subject headings: variable stars: RR Lyrae — galaxies: Local Group

1. INTRODUCTION

RR Lyrae variable stars have long been an important and useful tool for studying stellar populations. They are relatively easy to identify, given their narrow range of V magnitudes, short periods, and distinctive light curve shapes (at least for the RRab type). Their very presence is indicative of an old ($\gtrsim 10$ Gyr) stellar population and their pulsation properties (namely amplitudes and periods) can be used to find the metallicities and distances of their parent population.

Work on the RR Lyraes in the M31 system started in 1987 when Pritchett & van den Bergh used ground-based observations from the Canada-France-Hawaii Telescope to observe a field 9kpc from the galactic center. They identified 30 such stars with an estimated completeness of 25%. This same field was later observed by Dolphin et al. (2004) using the WIYN 3.5m at Kitt Peak. They found 24 RR Lyrae stars with an estimated completeness of $\sim 24\%$. Additional work has been done on RR Lyraes in the M31 spheroid (Sarajedini et al. 2009), M31 satellite galaxies M32 (Alonso-Garcia et al. 2004; Fiorentino et al. 2010) and M33 (Sarajedini et al. 2006), as well as

some of the globular cluster systems in M31 (Clementini et al. 2001; Contreras et al. 2008).

A comprehensive analysis of M31 RR Lyrae stars was enabled by ultra-deep imaging of a single field in the M31 halo, 11 kpc (51') from the nucleus (Brown et al. 2004, hereafter Paper I). In this study they utilized the excellent time coverage (250 exposures over 41 days, combining to ~ 84 hours of imaging time) afforded by a set of observations taken with the Wide Field Camera (WFC) channel of the Advanced Camera for Surveys (ACS) onboard the Hubble Space Telescope (HST). These data were taken to study the star formation history of this field by observing individual stars below the main sequence turn off (Brown et al. 2003). These observations, taken in both F606W (broad V) and F814W (I), did that, and they were able to construct a color magnitude diagram (CMD) of this field to an unprecedented depth ($V \sim 30.7$) with 100% completeness in the magnitude range of the RR Lyrae stars.

In this study we build upon and expand the work of Paper I. We have observed five more ultra deep fields in various regions of Andromeda, making six fields in total. These include observations of the disk, giant stellar stream, and several halo fields at varying distances from the galactic center (namely one at 21 kpc and two at 35 kpc), in addition to the halo field at 11 kpc. The completeness for star detection is $\sim 100\%$ at the magnitude level of the RR Lyrae stars. The identification of RR Lyrae stars within the stellar sample of each field is also $\sim 100\%$, due to the very high signal-to-noise ratio and excellent time sampling of the observations. In fact, it is worth noting that M31 RR Lyrae studies that employ HST observations with far less temporal coverage do not generally suffer from significant completeness issues (e.g., Sarajedini et al. 2009). As in Paper I, the

¹ Based on observations made with the NASA/ESA *Hubble Space Telescope*, obtained at STScI, which is operated by AURA, Inc., under NASA contract NAS 5-26555.

² Space Telescope Science Institute, 3700 San Martin Drive, Baltimore, MD 21218; jeffery@stsci.edu, edsmith@stsci.edu, tbrown@stsci.edu, jkalirai@stsci.edu, ferguson@stsci.edu,

³ Code 667, NASA Goddard Space Flight Center, Greenbelt, MD 20771; allen.v.sweigart@nasa.gov

⁴ University of California Observatories/Lick Observatory, Department of Astronomy & Astrophysics, University of California, Santa Cruz, CA 95064; raja@ucolick.edu

⁵ Osservatorio Astronomico, Vicolo Dell'Osservatorio 5, I-35122 Padova, Italy; alvio.renzini@oapd.inaf.it

⁶ Department of Physics and Astronomy, University of California, Los Angeles, CA 90095; rmr@astro.ucla.edu

Field	Dates	R.A.	Dec.	$n_{exp} \times \text{total (ks)}$	$n_{exp} \times \text{total (ks)}$
	Observed	(J2000)	(J2000)	(F606W)	(F814W)
disk	2004 Dec 11–2005 Jan 18	00 49 08.6	42 45 02	41 × 52.8	62 × 78.1
stream	2004 Aug 30–2004 Oct 4	00 44 18.2	39 47 32	41 × 52.8	62 × 78.1
halo11	2002 Dec 2–2003 Jan 1	00 46 07.1	40 42 39	108 × 138.6	126 × 161.3
halo21	2006 Aug 9–2006 Aug 28	00 49 05.1	40 17 32	24 × 28.7	40 × 47.8
halo35b	2006 Oct 18–2007 Jan 6	00 54 08.5	39 47 26	24 × 28.1	44 × 51.6

Table 1

Coordinates of the center of each observed field in M31, along with total number of exposures and combined exposure times in each filter. Units for right ascension are hours, minutes, seconds; units for declination are degrees, arcminutes, and arcseconds.

observations we describe here greatly surpass the requirements of a study strictly focused on M31 RR Lyrae stars, because the primary purpose of the observations was to investigate the star formation history in various fields of Andromeda. To that end, each region was observed with a long series of exposures to obtain photometry below the main sequence turn off (see Brown et al. 2006; 2007; 2008 for those results).

In the remainder of this paper, we will proceed as follows. We present a summary of the observations and data reductions in Section 2. In Section 3 we discuss our techniques for searching for the variable stars in the images, including identification of the RR Lyraes, as well as period determination and light curve fitting. We will discuss the properties of the samples of RR Lyrae stars in Section 4, including period distributions and Oosterhoff types. We discuss and compare various techniques to determine metallicities and distances in Section 5. We summarize findings and final conclusions in Section 6.

2. OBSERVATIONS AND DATA REDUCTION

As mentioned in Section 1, we obtained the data with HST/ACS with the primary goal of exploring the star formation histories of six fields in M31 by observing to an unprecedented depth, resolving stars below the main sequence turn off (see Brown et al. 2003; 2006; 2007; 2008). In Figure 1 we present the location of these fields on a map of the stellar densities in the vicinity of M31 (Ferguson et al. 2002). (We note that although the RR Lyraes in the 11kpc field have been discussed in Paper I, we include them in our analysis for completeness.) These observations represent over 300 HST orbits and 220.25 hours of imaging. The observations of each field (including central coordinate information and the number of individual exposures for each field) are summarized in Table 1. A more extensive description of these observations is given in Brown et al. (2009) and references therein.

A complete description of our data reduction process to search for variable stars is given in Paper I. In addition to the reductions and corrections described there, we also included corrections for charge transfer (in)efficiency (CTI, Chiaberge et al. 2009), as well as updated “breathing” corrections.

The halo11, stream and disk observations were performed early in the lifetime of the ACS/WFC CCD detector and those data were shown to be unaffected by CTI. The deep field photometry of the halo21 and both halo35 fields (Brown et al. 2008) included the best CTI corrections available at that time (Reiss & Mack 2004). Our photometry of the variables in those fields now employs the 2009 update to the CTI corrections (Chiaberge

et al. 2009). For stars as bright as horizontal branch (HB) RR Lyrae in our fields, the CTI correction ranges from near 0 to ~ 0.02 magnitudes.

Furthermore, the reductions now include a breathing correction – that is, an exposure by exposure correction for variation in focus of HST caused by orbital temperature variations (Makidon et al. 2006). We remove that variation’s effect on our aperture photometry, with an exposure by exposure normalization factor derived from the breathing induced variation in the mean brightness of a large number of red giant branch stars at \sim HB brightness.

3. CHARACTERIZATION OF THE VARIABLE STARS

3.1. Finding Variables

Our methods for searching for the variable stars in the fields is similar to that laid out in Paper I (see Section 3), with slight modification. To summarize, we first restricted our analysis to those stars brighter than $m_{F606W} = 28.28$, to include only stars with a signal-to-noise ratio > 5 . Only stars with at least 20 observations in F814W or 12 in F606W were included. We then computed the Lomb-Scargle periodogram (Lomb 1976; Scargle 1982) for each star in the catalog that met these criteria (regardless of position on the CMD). This algorithm searches for periodic signals in irregularly sampled data and quantifies its statistical significance. We accepted only stars with a score of less than 0.01, meaning that the chance that this signal arose from random noise is less than 1%. We relaxed this threshold to 2.5% for the two halo35 fields. We did not attempt to find stars again in the halo11 field.

As a second pass, we normalize the photometry of both bands by subtracting their median magnitude and then scale the F606W values by 0.7, the approximate I/V ratio of RR Lyrae amplitudes. We then combine the scaled F606W values with F814W. This improves the time sampling in order to find additional RR Lyrae stars that may have been missed during the first pass. This typically yielded no more than one or two more RR Lyrae stars in a given field.

We found RR Lyraes in five of the six ultra deep fields examined. As noted in Paper I, there are 55 in the halo11 field. In addition to these, we found RR Lyrae stars in the other fields as follows: 21 in the disk, 24 in the stream, 3 in halo22, none in halo35a, and five in halo35b. We note that we found no RR Lyrae stars in the halo35a field. This was not a surprise, given the low stellar density (roughly 1:3) compared to the halo21 field where we found three RR Lyrae stars. We may have expected to find a similar number of RR Lyrae stars in the halo35a field as compared to the halo35b field (where we found

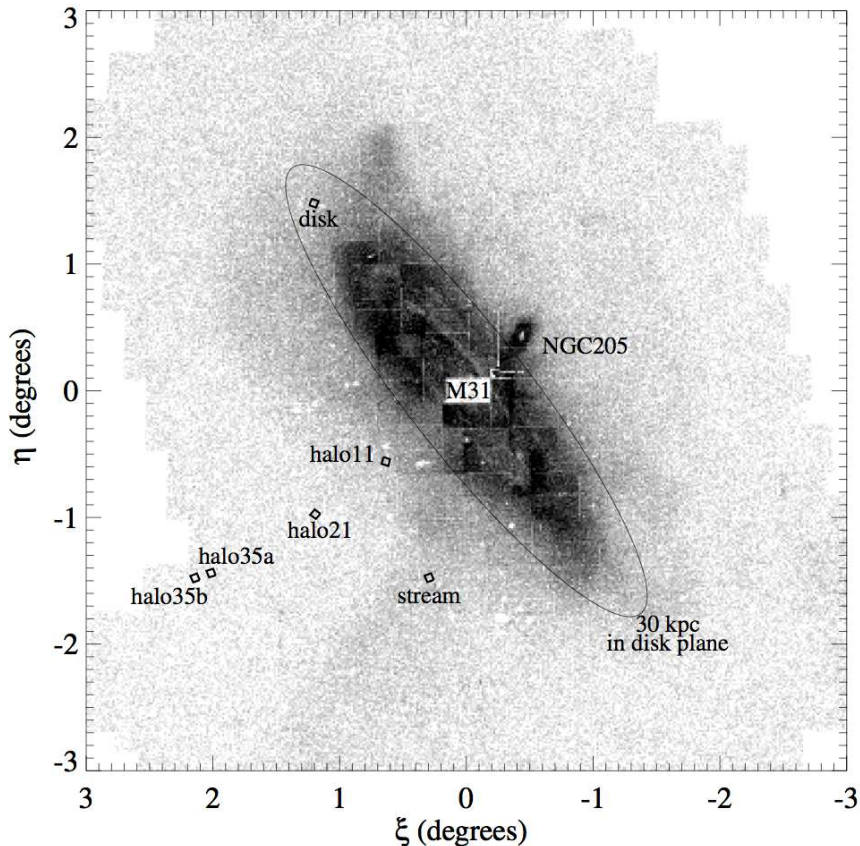


Figure 1. A map of stellar density (from Ferguson et al. 2002) in the vicinity of M31 with our six fields indicated. The ellipse marks the area within 30 kpc of the galactic center in the inclined plane (as labeled). Figure taken from Brown et al. (2009).

five RR Lyraes), as the two fields have nearly equal stellar density. Thus we thoroughly re-examined our processing and variable finding analysis of the halo35a data. Still finding no RR Lyrae, we added an additional search method. We processed the photometry of all, ~ 60 , stars in or near the RR Lyrae region of the CMD with the template fitting program (see Section 3.2). This still yielded null results. We are therefore confident in the lack of RR Lyraes in this field.

We have included a complete list of the number of RR Lyraes, the ratio of c-type to the total number of RR Lyraes in each field, and average periods of each type for each field in Table 2. For comparison, we have also listed the corresponding values for the Milky Way (MW) globular clusters (GCs) of Oosterhoff (1939) types I and II (from Clement et al. 2001).

We indicate the positions of the RR Lyrae stars (and Cepheids, when found, see Section 3.3) on the CMD of each field in Figures 2 through 5. We refer the reader to Paper I for the CMD of the halo11 field. The photometry of the CMDs is from Brown et al. (2009). The photometry for the RR Lyraes is based on the average magnitude and color found by light curve template fitting (as explained below). In these figures, the top panel represents the CMD of the entire field, while the lower panel is a region zoomed to include just the RR Lyrae region on the horizontal branch (as indicated by the gray box in the top panel). In these figures, we represent the ab-type RR Lyraes with crosses, while the c-type variables are open triangles.

To help us understand the reliability and completeness

of our finding routine, we created artificial light curves to process and determine the fraction that were successfully recovered. These synthetic light curves had average F606W and F814W magnitudes comparable to our real data and were created with a combination of all periods between 0.2 and 1.0 days (in increments of 0.1 days), and all F814W amplitudes between 0.1 and 1.5 magnitudes (in increments of 0.1, and scaling the corresponding synthetic F606W amplitudes accordingly). We then sampled these synthetic light curves according to the time sampling of our fields. We used the modified Julian date (MJD) values for the stream and the halo21 fields, and expect similar results for the disk and both halo35 fields,

Field	Total		$\langle P_{ab} \rangle$	$\langle P_c \rangle$
	RR Lyrae	N_{RRc}/N_{RRtot}		
disk	21	0.43	0.583	0.341
stream	24	0.33	0.560	0.336
halo11	55	0.47	0.594	0.318
halo21	3	0.00	0.599	–
halo35a	0	–	–	–
halo35b	5	0.40	0.495	0.359
MW GC OoI	–	0.22	0.559	0.326
MW GC OoII	–	0.48	0.659	0.368

Table 2

Summary of the properties of the RR Lyraes in our M31 fields. Properties of the Milky Way globular clusters (MW GC) of Oosterhoff type I and II (Clement et al. 2001) are included for comparison. The last three columns indicate the ratio of RRc to total RR Lyrae stars, the average period for the ab-type stars, and the average period for the c-type stars.

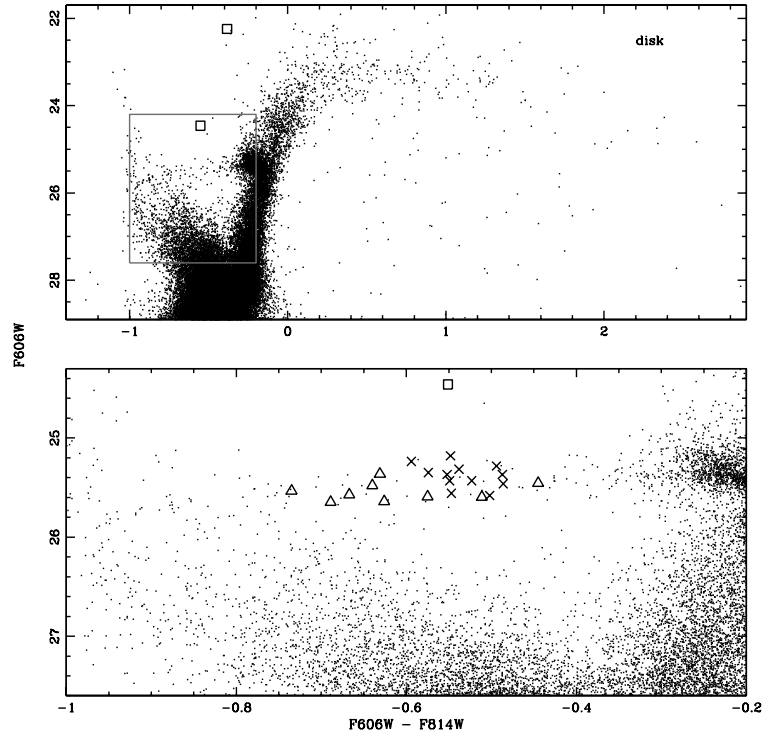


Figure 2. Top: CMD of the M31 disk field from Brown et al. (2009). The Cepheids found in this field are marked as open squares. The gray box indicates the subsection of the CMD displayed in the bottom panel. Bottom: Expanded view of the CMD and positions of the RR Lyraes on the horizontal branch. RRab stars are indicated with crosses and RRc stars with the open triangles.

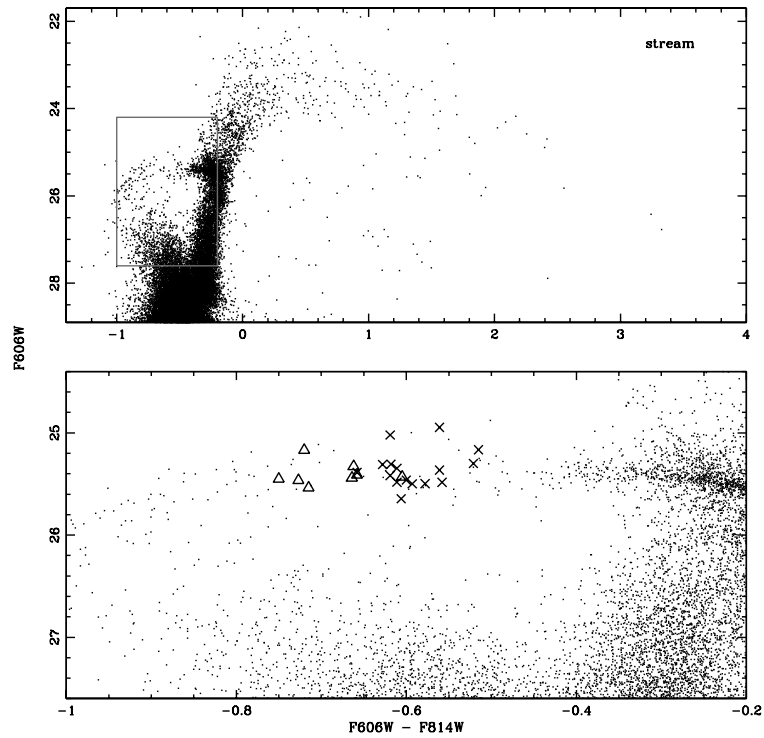


Figure 3. Same as Figure 2, but for the stream field.

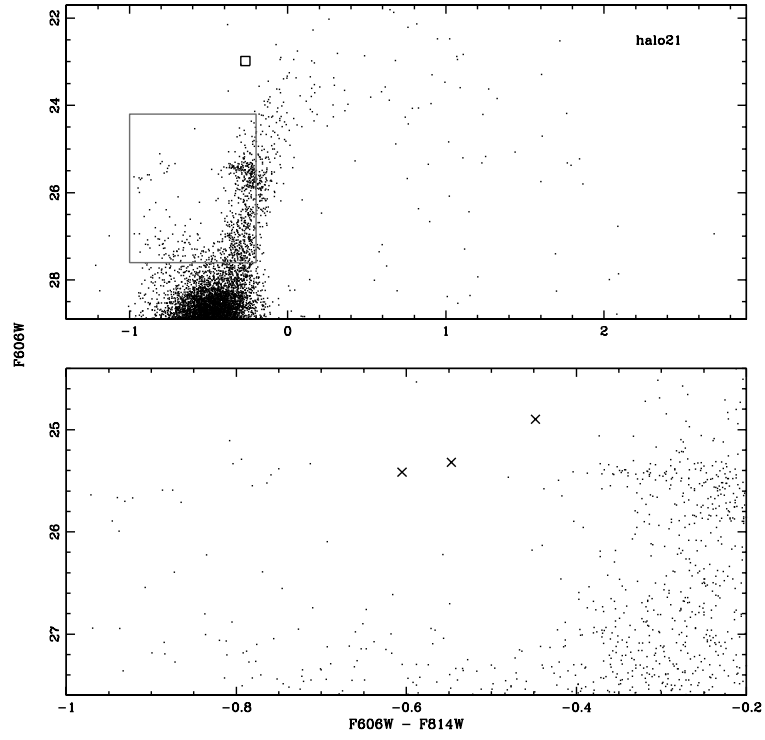


Figure 4. Same as Figure 2, but for the halo21 field.

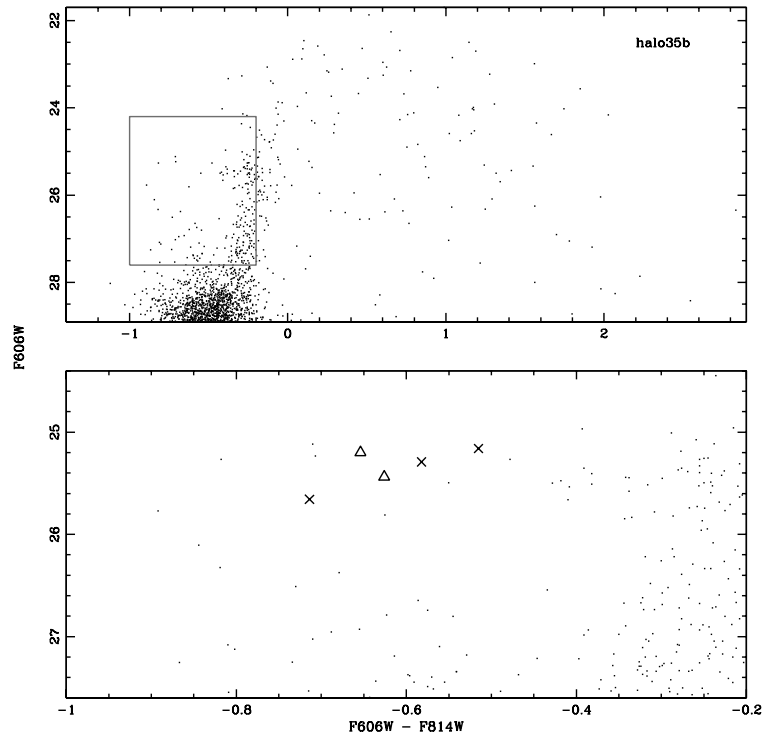


Figure 5. Same as Figure 2, but for the halo35b field.

respectively, as the time sampling is similar. We then scattered individual synthetic photometry values with random Gaussian errors, according to the errors of the photometry in our real data.

We input these simulated light curves into our finding algorithm. For time sampling similar to the stream and disk fields, 100% of the synthetic stars were recovered. For the less frequently sampled halo21 and halo35 fields, 97% were still recovered. We note that of the 3% of the stars that were not recovered in this instance, most had very small amplitudes (0.1 magnitudes). Because of this, we are confident that our finding routine is indeed able to find all the RR Lyraes that are present in these fields.

Once we have a list of candidate RR Lyraes in our fields from our finding routine, we are ready to determine exact periods and amplitudes.

3.2. Periods and Light Curve Fitting

Once the RR Lyrae candidates in our M31 fields were identified as described in the previous section, we determined their periods and other pulsation properties. Because the RR Lyraes in the halo11 field were so well sampled in time, in Paper I we used high order polynomials to fit the light curves. However, as can be seen from Table 1, subsequent observations of the other ultra deep fields consisted of increasingly sparser observations. While this did not appreciably affect the completeness level of the observations of RR Lyrae stars, it did affect the reliability of the polynomial fits. To mitigate this, we employed a light curve template fitting program, specifically designed for RR Lyrae stars.

We used the program FITLC⁷ (Sarajedini et al. 2009) to determine periods and fit template light curves to the data. This template-fitting, period-finding algorithm is a reincarnation of the FORTRAN code written for the Layden & Sarajedini (2000) study, rewritten using the Interactive Data Language (IDL), incorporating a graphical user interface (GUI). The algorithm uses 10 template light curves: six ab-type RR Lyraes, two c-type RR Lyraes, one eclipsing binary, and one contact binary. It searches over a user-specified period range in user-specified period increments, looking for the fit that minimizes the χ^2 value, simultaneously fitting multiple filters, as available. In addition to the period, FITLC also returns the amplitude and mean magnitude of the star in each filter.

When running FITLC on an individual RR Lyrae star, we first set the period to search over the default period range and increment, namely 0.2 to 1.0 day at 0.01 day increments. This returned a good estimate of the period. From there, we refined the search to find a more precise fit by decreasing the period range and increment, until a period was found to five decimal places (i.e., the period increment was equal to 10^{-5} day). We note that for consistency in our analysis we also fit stars in the halo11 field using FITLC. Both the polynomial fits in Paper I and the present template fit gave comparable results. The consistency of the two methods for period fitting is indicative of the reliability of FITLC to providing high quality fits for RR Lyrae light curves.

In Tables 3 to 6 we list the individual photometry values for the RR Lyraes in each field, excluding the halo11

MJD	Filter	987	987 (err)	1741	1741 (err)	...
53350.176	F814W	26.213	0.045	25.708	0.031	...
53350.192	F814W	26.227	0.047	25.678	0.032	...
53350.236	F814W	26.163	0.044	25.822	0.034	...
⋮	⋮	⋮	⋮	⋮	⋮	⋮

Table 3

Photometry of RR Lyrae stars in the disk. The modified Julian day (MJD) is for the middle of the observation. This table is available in its entirety in machine-readable form in the online journal. A portion is shown here for guidance regarding its form and content.

MJD	Filter	409	409 (err)	561	561 (err)	...
53247.604	F606W	99.000	9.000	25.777	0.035	...
53247.620	F606W	99.000	9.000	25.792	0.038	...
53247.668	F606W	99.000	9.000	25.767	0.033	...
⋮	⋮	⋮	⋮	⋮	⋮	⋮

Table 4

Same as Table 3, except for the stream.

MJD	Filter	3520	3520 (err)	6221	6221 (err)	...
53956.860	F606W	25.508	0.030	24.883	0.041	...
53956.909	F606W	25.639	0.032	24.873	0.039	...
53956.924	F606W	25.625	0.033	24.871	0.039	...
⋮	⋮	⋮	⋮	⋮	⋮	⋮

Table 5

Same as Table 3, except for the halo21 field.

MJD	Filter	2083	2083 (err)	2299	2299 (err)	...
54026.517	F814W	99.999	9.999	25.502	0.030	...
54026.533	F814W	99.999	9.999	25.522	0.031	...
54026.584	F814W	25.928	0.039	25.603	0.031	...
⋮	⋮	⋮	⋮	⋮	⋮	⋮

Table 6

Same as Table 3, except for the halo35b field.

field. We refer the reader to Paper I for these data. Tables 7 to 11 list the properties of each RR Lyrae star in each field, including period, amplitude, and intensity-weighted mean magnitude for each filter (as calculated by FITLC). Light curves for the individual RR Lyrae stars in each field (except for the halo11 field, see Paper I) are displayed in Figures 6 through 9, in order of increasing period with the best fit template light curve overplotted. Error bars are also plotted. The dark gray points are observations in F606W while the light gray points are F814W.

⁷ <http://www.mancone.net/fitlc/index.php>

Name	R.A. (J2000)	Dec. (J2000)	Period (days)	m_{F606W} (mag)	m_{F814W} (mag)	A_{F606W} (mag)	A_{F814W} (mag)	Type
15256	00 49 14.96	42 44 09.4	0.2536	25.535	26.274	0.349	0.219	c
20444	00 49 15.28	42 46 25.6	0.2920	25.479	26.127	0.447	0.266	c
17168	00 49 13.20	42 45 48.4	0.2950	25.646	26.341	0.473	0.330	c
19576	00 49 13.13	42 46 57.4	0.3052	25.573	26.246	0.466	0.336	c
21631	00 49 13.97	42 45 10.2	0.3212	25.457	25.908	0.383	0.200	c
18504	00 49 13.78	42 46 10.1	0.3371	25.366	26.001	0.390	0.262	c
8247	00 49 06.63	42 44 41.0	0.3554	25.641	26.275	0.473	0.257	c
987	00 48 58.78	42 45 04.5	0.3979	25.588	26.102	0.408	0.307	c
20858	00 49 01.69	42 43 44.4	0.4471	25.476	26.082	1.109	0.747	ab
4302	00 49 03.49	42 44 23.3	0.5121	25.595	26.167	0.250	0.352	c
17280	00 49 13.00	42 45 56.8	0.5243	25.347	25.966	0.960	0.643	ab
8697	00 49 06.89	42 44 46.5	0.5330	25.607	26.173	0.857	0.550	ab
7941	00 49 07.09	42 44 21.5	0.5339	25.480	26.054	0.896	0.572	ab
21601	00 49 15.38	42 44 12.4	0.5402	25.448	26.009	1.031	0.710	ab
15534	00 49 15.30	42 44 08.8	0.5846	25.470	26.026	0.535	0.386	ab
20204	00 49 17.83	42 45 12.9	0.5892	25.664	26.178	0.626	0.406	ab
1741	00 49 00.12	42 44 47.6	0.6297	25.318	25.817	0.483	0.330	ab
16135	00 49 11.08	42 46 15.1	0.6334	25.489	25.977	0.330	0.226	ab
15853	00 49 09.65	42 46 43.9	0.6368	25.236	25.799	0.858	0.605	ab
11181	00 49 12.19	42 43 32.7	0.6571	25.409	25.904	0.567	0.375	ab
10949	00 49 07.54	42 45 26.8	0.6880	25.462	25.988	0.403	0.309	ab

Table 7
Properties of the RR Lyrae stars found in the disk.

Name	R.A. (J2000)	Dec. (J2000)	Period (days)	m_{F606W} (mag)	m_{F814W} (mag)	A_{F606W} (mag)	A_{F814W} (mag)	Type
409	00 44 26.91	39 48 40.1	0.2702	25.462	26.190	0.257	0.216	c
7343	00 44 20.90	39 47 06.0	0.2967	25.535	26.259	0.516	0.355	c
8544	00 44 09.84	39 47 35.8	0.3030	25.453	26.204	0.134	0.108	c
5414	00 44 16.66	39 48 02.3	0.3467	25.434	26.101	0.359	0.256	c
9016	00 44 14.07	39 47 06.2	0.3517	25.327	25.996	0.478	0.300	c
649	00 44 18.66	39 49 14.6	0.3584	25.411	26.077	0.425	0.197	c
9975	00 44 23.53	39 46 03.9	0.3666	25.168	25.889	0.209	0.150	c
5600	00 44 16.43	39 47 60.0	0.3955	25.423	26.031	0.350	0.260	c
3674	00 44 22.49	39 48 06.3	0.4550	25.531	26.219	1.175	0.830	ab
8851	00 44 12.10	39 47 19.6	0.4738	25.487	26.124	1.118	0.797	ab
8877	00 44 15.83	39 47 01.3	0.4899	25.561	26.217	1.177	0.699	ab
10510	00 44 10.67	39 46 52.8	0.4946	25.446	26.092	1.122	0.777	ab
2838	00 44 19.31	39 48 35.3	0.5071	25.452	26.108	1.147	0.805	ab
2577	00 44 17.16	39 48 49.2	0.5081	25.789	26.432	1.186	0.732	ab
561	00 44 13.40	39 49 40.7	0.5314	25.550	26.175	0.805	0.559	ab
7671	00 44 18.20	39 47 12.5	0.5315	25.570	26.179	0.886	0.636	ab
1669	00 44 25.27	39 48 26.0	0.5583	25.542	26.191	1.271	0.697	ab
8458	00 44 22.24	39 46 39.4	0.5803	25.532	26.100	0.665	0.469	ab
10614	00 44 09.82	39 46 54.6	0.6050	25.143	25.791	1.037	0.682	ab
2715	00 44 20.02	39 48 33.8	0.6060	25.527	26.108	0.379	0.266	ab
721	00 44 14.81	39 49 31.3	0.6083	25.423	25.997	0.669	0.386	ab
7874	00 44 22.06	39 46 51.3	0.6192	25.028	25.597	0.586	0.412	ab
2933	00 44 26.76	39 47 59.2	0.6694	25.196	25.714	0.399	0.253	ab
4433	00 44 23.96	39 47 46.7	0.7277	25.334	25.859	0.472	0.349	ab

Table 8
Properties of the RR Lyrae stars found in the stream.

Name	R.A. (J2000)	Dec. (J2000)	Period (days)	m_{F606W} (mag)	m_{F814W} (mag)	A_{F606W} (mag)	A_{F814W} (mag)	Type
V130	00 46 11.91	40 42 45.1	0.2628	25.638	26.365	0.447	0.317	c
V89	00 46 06.68	40 43 21.9	0.2670	25.523	26.258	0.412	0.291	c
V76	00 46 05.86	40 42 52.9	0.2743	25.422	26.140	0.148	0.114	c
V100	00 46 06.94	40 43 58.7	0.2746	25.579	26.281	0.465	0.311	c
V137	00 46 11.13	40 43 48.8	0.2804	25.595	26.280	0.337	0.218	c
V120	00 46 12.78	40 41 24.6	0.2830	25.381	26.104	0.485	0.324	c
V27	00 45 57.64	40 43 33.5	0.2870	25.639	26.314	0.475	0.286	c
V40	00 46 01.20	40 42 19.8	0.2886	25.396	26.139	0.162	0.100	c
V102	00 46 08.57	40 43 10.5	0.3008	25.504	26.208	0.446	0.288	c
V37	00 46 03.26	40 40 39.9	0.3012	25.473	26.150	0.452	0.315	c
V8	00 46 01.02	40 40 44.1	0.3055	25.603	26.264	0.362	0.285	c
V163	00 46 15.92	40 42 37.9	0.3126	25.342	26.008	0.359	0.200	c
V80	00 46 05.78	40 43 28.8	0.3135	25.500	26.208	0.426	0.288	c
V131	00 46 13.72	40 41 30.6	0.3266	25.498	26.143	0.373	0.219	c
V157	00 46 16.21	40 41 47.6	0.3291	25.462	26.160	0.409	0.287	c
V161	00 46 13.32	40 44 18.7	0.3301	25.550	26.180	0.343	0.271	c
V11	00 45 56.88	40 43 44.1	0.3307	25.619	26.215	0.418	0.322	c
V43	00 46 01.74	40 42 20.6	0.3379	25.361	26.032	0.507	0.319	c
V5	00 46 00.61	40 40 52.4	0.3386	25.543	26.166	0.383	0.310	c
V59	00 46 03.80	40 42 36.9	0.3388	25.450	26.111	0.425	0.286	c
V83	00 46 08.84	40 41 35.5	0.3515	25.336	26.026	0.491	0.320	c
V90	00 46 07.71	40 42 51.1	0.3533	25.495	26.128	0.434	0.233	d
V95	00 46 09.60	40 41 39.8	0.3616	25.409	26.046	0.363	0.242	c
V54	00 46 04.33	40 41 35.2	0.3659	25.402	26.053	0.390	0.273	c
V50	00 46 02.68	40 42 31.0	0.3660	25.457	26.119	0.469	0.287	c
V1	00 45 59.76	40 41 18.2	0.3816	25.364	25.989	0.377	0.276	c
V147	00 46 11.66	40 44 23.3	0.4417	25.462	26.090	1.044	0.633	ab
V44	00 45 59.93	40 43 38.9	0.4641	25.625	26.258	1.036	0.729	ab
V47	00 46 01.55	40 42 44.8	0.4958	25.519	26.120	1.083	0.757	ab
V88	00 46 09.86	40 41 03.5	0.5056	25.517	26.125	1.049	0.770	ab
V79	00 46 04.60	40 44 09.8	0.5289	25.456	26.039	1.102	0.773	ab
V28	00 46 00.08	40 42 02.9	0.5322	25.559	26.118	0.846	0.621	ab
V162	00 46 16.08	40 42 25.4	0.5332	25.535	26.124	0.919	0.668	ab
V126	00 46 10.38	40 43 32.5	0.5337	25.433	26.034	0.941	0.583	ab
V42	00 46 00.77	40 43 00.9	0.5519	25.308	25.884	1.040	0.731	ab
V57	00 46 02.60	40 43 10.6	0.5544	25.379	25.978	1.021	0.687	ab
V142	00 46 11.47	40 44 04.1	0.5545	25.378	25.958	0.913	0.636	ab
V140	00 46 14.51	40 41 37.0	0.5587	25.325	25.935	1.092	0.820	ab
V133	00 46 13.43	40 41 54.5	0.5717	25.339	25.927	0.859	0.646	ab
V112	00 46 11.88	40 41 21.5	0.5729	25.374	25.973	0.941	0.572	ab
V164	00 46 14.21	40 43 55.8	0.5802	25.429	25.991	0.833	0.571	ab
V166	00 46 13.71	40 44 24.4	0.5825	25.443	25.978	0.665	0.550	ab
V122	00 46 13.10	40 41 14.2	0.5886	25.319	25.946	0.810	0.478	ab
V160	00 46 14.30	40 43 22.7	0.6115	25.245	25.802	0.722	0.472	ab
V167	00 46 10.38	40 43 44.0	0.6214	25.402	25.941	0.603	0.413	ab
V124	00 46 09.88	40 43 34.7	0.6265	25.342	25.876	0.703	0.530	ab
V36	00 46 02.04	40 41 29.0	0.6274	25.280	25.887	1.017	0.656	ab
V123	00 46 12.46	40 41 42.2	0.6314	25.254	25.813	0.659	0.478	ab
V136	00 46 10.23	40 44 23.2	0.6342	25.543	26.064	0.472	0.314	ab
V77	00 46 04.22	40 44 05.8	0.6783	25.508	26.029	0.590	0.427	ab
V10	00 46 00.68	40 41 02.9	0.6872	25.138	25.717	0.931	0.662	ab
V66	00 46 04.71	40 42 32.6	0.7130	25.356	25.855	0.535	0.300	ab
V114	00 46 10.11	40 42 54.5	0.7249	25.296	25.796	0.343	0.242	ab
V82	00 46 05.29	40 44 02.4	0.7350	25.457	25.991	0.527	0.334	ab
V78	00 46 08.34	40 41 24.6	0.7748	25.365	25.912	0.507	0.361	ab

Table 9
Properties of RR Lyrae stars found in the halo11 field.

Name	R.A. (J2000)	Dec. (J2000)	Period (days)	m_{F606W} (mag)	m_{F814W} (mag)	A_{F606W} (mag)	A_{F814W} (mag)	Type
3520	00 49 04.97	40 19 24.4	0.5141	25.491	26.096	0.626	0.465	ab
11608	00 49 01.09	40 17 47.8	0.6341	25.367	25.924	0.843	0.668	ab
6221	00 49 11.22	40 17 05.4	0.6497	24.914	25.361	0.305	0.171	ab

Table 10
Properties of RR Lyrae stars found in the halo21 field.

Name	R.A. (J2000)	Dec. (J2000)	Period (days)	m_{F606W} (mag)	m_{F814W} (mag)	A_{F606W} (mag)	A_{F814W} (mag)	Type
3053	00 54 01.43	39 46 20.5	0.3490	25.411	26.024	0.255	0.233	c
7085	00 54 15.97	39 44 18.4	0.3650	25.724	26.439	0.551	0.148	ab
4616	00 54 07.35	39 45 23.3	0.3680	25.174	25.830	0.445	0.272	c
2083	00 53 58.01	39 46 47.1	0.5030	25.376	25.970	0.792	0.576	ab
2299	00 53 58.77	39 46 41.3	0.6164	25.193	25.711	0.663	0.512	ab

Table 11
Properties of RR Lyrae stars found in the halo35b field.

To test the period and light curve type determination of FITLC, we took the same set of synthetic light curves described in Section 3.1 and processed them through FITLC. The results were excellent; the average period difference was less than 0.0001 days. The light curve type was correctly identified for 99.9% of the stars for ab-type and for 99.3% of the c-type. (We note that we counted an identification as correct as long as any template for the correct type provided the lowest χ^2 value.) This reinforces our confidence in the results of FITLC.

3.3. Cepheids

In addition to the RR Lyraes, our search for variable stars has yielded three Cepheids: two in the disk (star 13779 and star 5917) and one in the halo21 field (star 12571). We have marked these stars on the appropriate CMDs with open squares (see Figures 2 and Figure 4). In Tables 12 and 13 we list the individual photometry values for these Cepheids. We plot the phased light curve in both F606W and F814W in Figure 10, and note their periods. The star 5917 in the disk appears to be an anomalous Cepheid (Zinn & Searle 1976), with a (relatively) short period ($P \sim 0.5501$ days) and a magnitude brighter than the RR Lyrae stars.

We list the properties of these Cepheids, including coordinate information, in Table 14.

4. RR LYRAE PROPERTIES

Here we discuss the various properties of the RR Lyrae population in each field. This includes the period distribution, the Oosterhoff type, and reddening.

MJD	Filter	5917	5917 (err)	13779	13779 (err)
53350.176	F814W	25.411	0.027	22.775	0.007
53350.192	F814W	24.799	0.019	22.782	0.007
53350.236	F814W	25.291	0.026	22.759	0.006
⋮	⋮	⋮	⋮	⋮	⋮

Table 12

Photometry of the two Cepheids found in the disk field. This table is available in its entirety in machine-readable form in the online journal. A portion is shown here for guidance regarding its form and content.

4.1. Period Distribution

In Figure 11 we display the period distribution of the stars in each of the fields; RRab stars are represented with the thin lines while the RRc stars are indicated by the thick lines. As expected, the two types of RR Lyrae stars separate from each other. In this figure we have indicated the average periods for both types, and indicated these with the vertical dashed lines.

We note the presence of two seeming outliers in the period distributions for their respective type: the star 4302 (a c-type star with an unusually long period) in the disk, and the star 7085 (an ab-type star with an unusually short period) in the halo35b field. In the examination of 4302, we noted two high points in the F814W band photometry (near phase 0.0 and replotted at 1.0, see Figure 6), leading us to question the c-type fit as correct. We investigated if these two points were indicative of the familiar saw-tooth shape of the ab-type. A check of the star on the individual images did not indicate any anomalous cosmic ray hits, hot pixels, or contamination from a nearby star. However, given the higher quality fit to the c-type template when compared to the RRab template, and comparing the fit of the photometry on the light curve both immediately preceding and following these two points, we are convinced that the classification of 4302 as a c-type is correct. This is interesting, given its relatively long period, though we are unsure why this particular population would form such a star. Long period c-types are defined as having periods longer than 0.45^d (Contreras et al. 2005), and only a few of these stars have been found in MW GCs, including ω Cen, NGC 6388, NGC 6441, and M3 (Catelan 2004).

MJD	Filter	12571	12571 (err)
53956.860	F606W	22.843	0.007
53956.909	F606W	22.771	0.007
53956.924	F606W	22.851	0.007
⋮	⋮	⋮	⋮

Table 13

Same as Table 12, but for the Cepheid in the halo21 field.

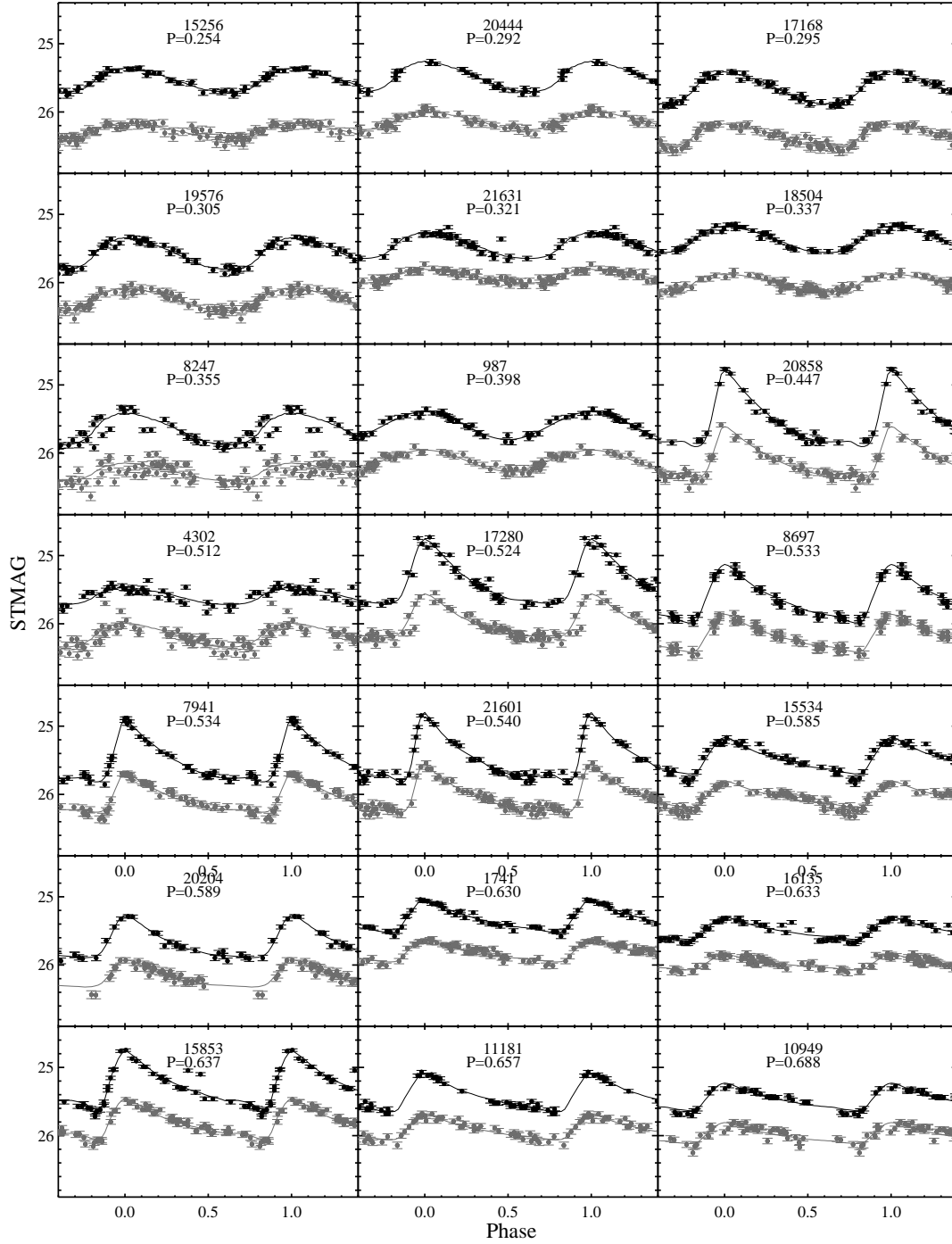


Figure 6. Phased light curves of RR Lyrae stars in the disk, arranged in order of increasing period. Error bars are included, and the best fit RR Lyrae template light curve is also plotted. The dark points are observations in F606W, while the light gray points are in F814W.

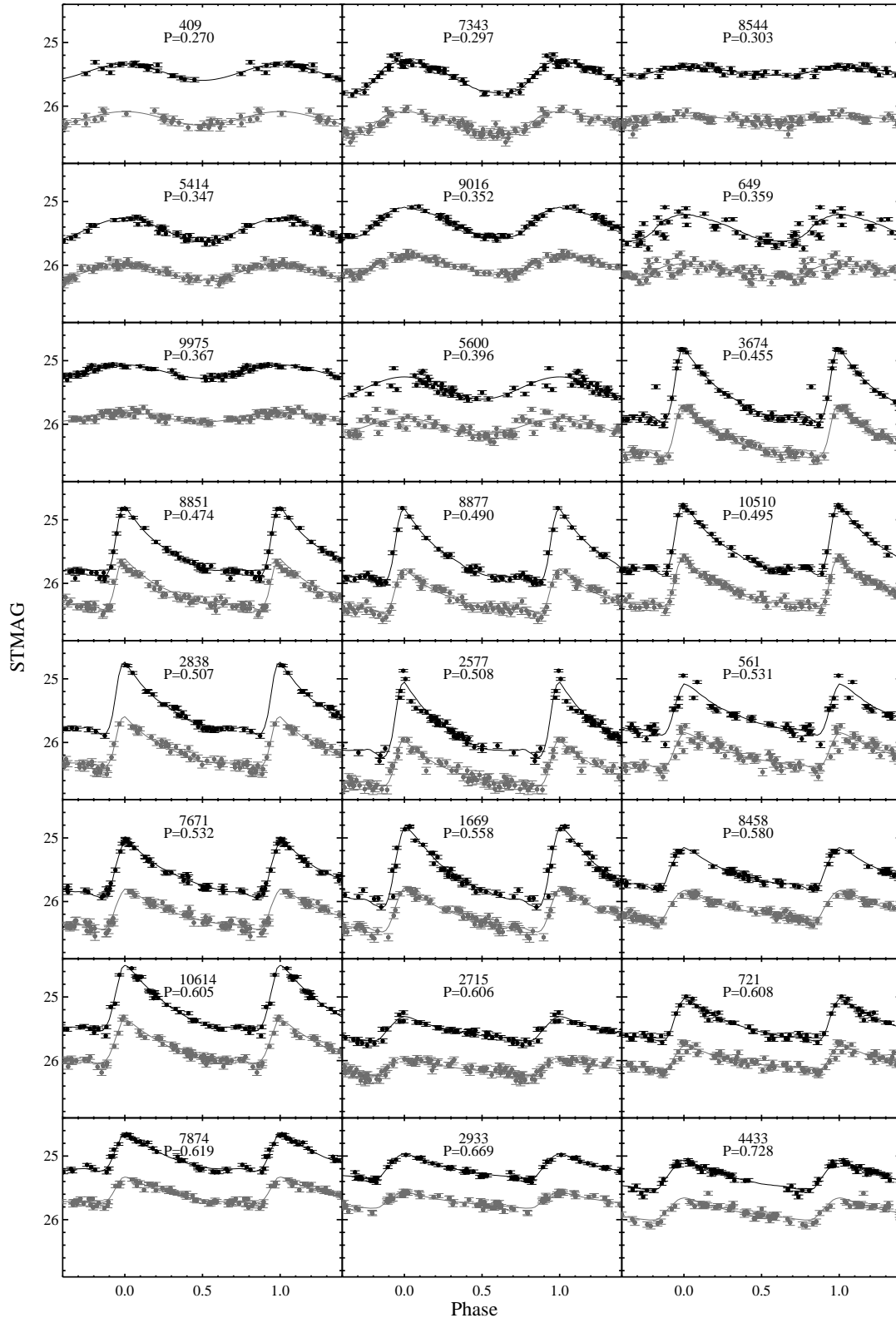


Figure 7. Same as Fig. 6, but for the stream field RR Lyraes.

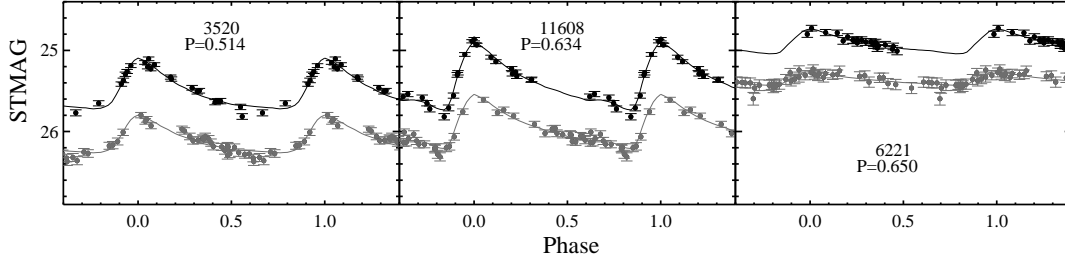


Figure 8. Same as Fig. 6, but for the halo21 field RR Lyraes.

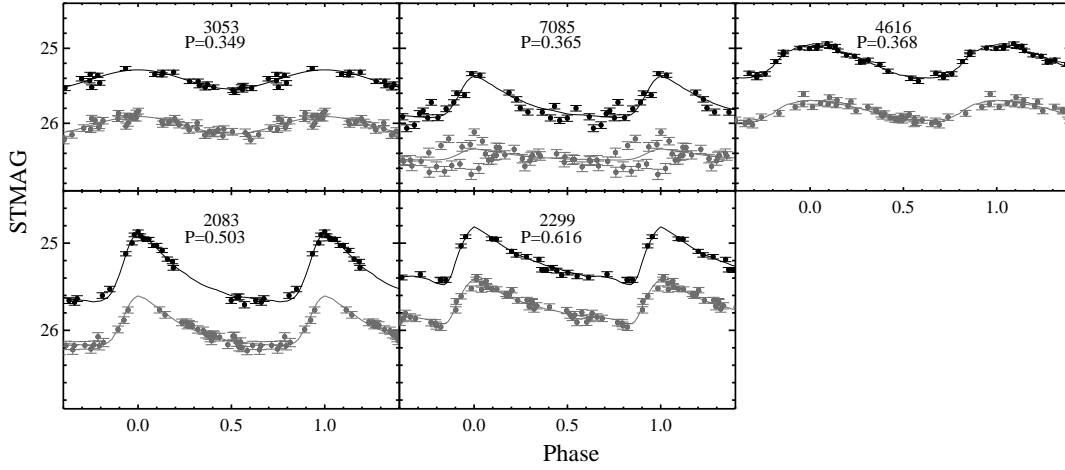


Figure 9. Same as Fig. 6, but for the halo35b field RR Lyraes.

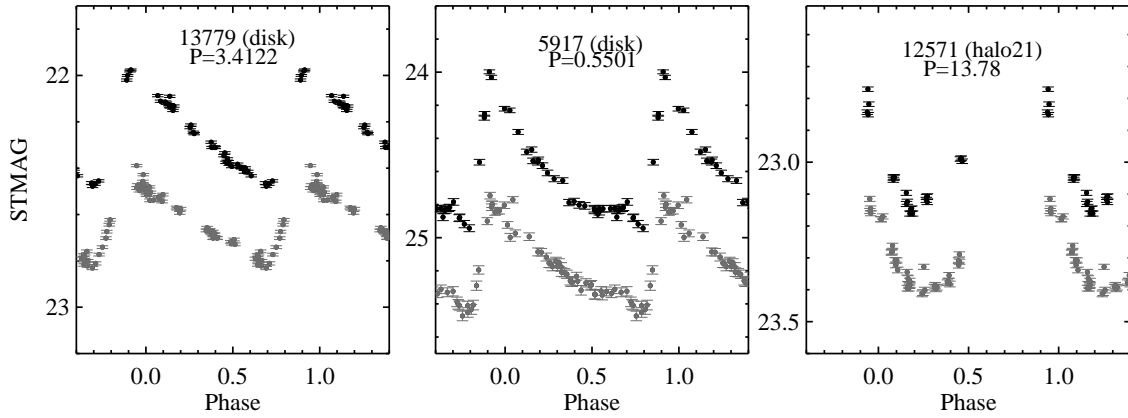


Figure 10. Phased light curves for the three Cepheids found in our sample. Periods (in days) are listed for each star.

Name	R.A. (J2000)	Dec. (J2000)	Period (days)	m_{F606W} (mag)	m_{F814W} (mag)	A_{F606W} (mag)	A_{F814W} (mag)	Field
5719	00 49 04.67	42 44 33.4	0.5501	24.615	25.168	0.941	0.659	disk
13779	00 49 10.54	42 45 25.9	3.4122	22.245	22.628	0.502	0.383	disk
12571	00 49 06.74	40 16 07.0	13.78	22.985	23.252	0.359	0.323	halo21

Table 14
Properties of the Cepheids found in our fields.

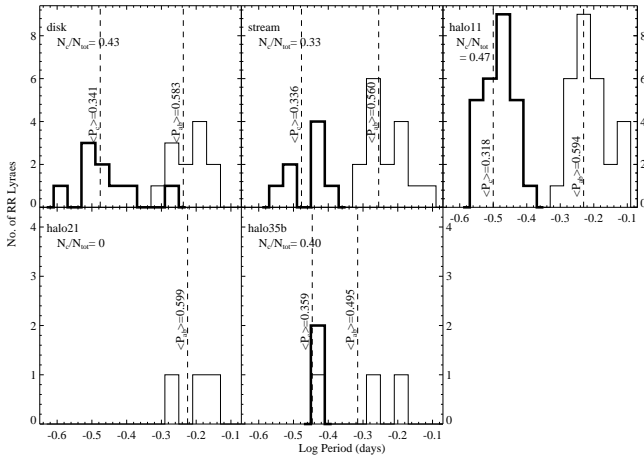


Figure 11. Period distributions of RR Lyrae stars in our five M31 fields where these stars were found. RRab stars are indicated with thin lines while the RRc stars are the thick lines. The average of the distributions of each type is indicated by the dashed vertical lines; the ratio of c-type to total RR Lyraes is also indicated.

It remains unclear as to why some populations can produce long period c-types, while others do not. It is interesting to note that the Galactic GCs with long-period RRc stars (listed above), are among the most massive GCs in the Milky Way. Additionally, the CMD morphology of these clusters indicates the presence of multiple populations (e.g., Bedin et al. 2004; Rich et al. 1997; Piotto et al. 2002). Analysis of multiple main sequences in ω Cen, for example, show the helium abundance (Y) in the cluster may have also changed drastically from one star formation episode to the next (Piotto et al. 2005). Interestingly, in studying different scenarios possibly responsible for bimodal horizontal branches in the massive GCs NGC 6388 and NGC 6441, Yoon et al. (2008) found that the super-helium-rich scenario would lead to c-types of longer periods. (These two particular clusters, however, also exhibit other strange properties, including an unusually high average period for RRab type stars, and not fitting into either Oosterhoff type; see Pritzl et al. 2000 for more details). However, tests of the horizontal branch morphology of M3 show no signs of helium enrichment (Catelan et al. 2009). While these explanations are intriguing, it remains unclear as to the true explanation for these long period c-types, and the significance, if any, of the presence of one in our disk field.

Second, we note star 7085 ($P=0.365^d$) in the halo35b field. Initially we investigated if this star’s short period would place it among the c-type stars. However, the ab-type template is a higher quality fit (see especially the fit to the F606W data in Figure 9), and we note the existence of a handful of ab-type RR Lyraes with similarly short periods in other studies (e.g., Sarajedini et al. 2009). We note the scatter in the F814W band (see Figure 9). Although some data points in the F814W band cover a much larger time range than the F606W (i.e., of order 80 days), the exclusion of these points does not increase the quality of the fit. This indicates that the scatter is not the result of the Blazhko effect (Blazhko 1907). This star is fainter than the other RR Lyraes in this field, so it could be simply the result of increased photometric scatter (although the error bars are small).

Because of our limited information we leave the classification as it is, and proceed with our analysis.

4.2. Oosterhoff Type

Oosterhoff (1939) noticed similarities among RR Lyraes in different globular clusters (GCs) in the Milky Way and subsequently classified these variables into two classes, Type I and Type II (often denoted as OoI and OoII, respectively). OoI GCs tend to have a smaller ratio of c-type to total RR Lyraes, with shorter average periods, and hence more metal rich compared to the OoII GCs. The two types also occupy different regions of the Bailey diagram, a plot of the amplitude vs. the logarithm of the period for individual stars. The so-called Oosterhoff gap is the gap between these two types, especially evident in a plot of period shift (shifted relative to M3 RR Lyrae stars) versus metallicity (e.g., Suntzeff, Kinman, & Kraft 1991, see especially their Figure 8). RR Lyraes in the Milky Way field, while more difficult to characterize than those in the GCs, seem to show a higher tendency toward the OoI type (Cacciari & Renzini 1976), and still exhibit the Oosterhoff gap.

Recent studies of RR Lyrae stars in dwarf spheroidal (dSph) satellite galaxies of the Milky Way reveal that these stars populate an intermediate Oosterhoff type, bridging the Oosterhoff gap (Siegel & Majewski 2000). Similarly, this intermediate Oosterhoff type has been observed in the M31 halo (Paper I) and M31 dSph galaxies (e.g., And VI, Pritzl et al. 2002) However, some objects in the M31 system do not show this intermediate behavior; for example, two spheroidal fields of M31 near M32 are of OoI type (Sarajedini et al. 2009).

Initial classification of the stars in these fields as either Oosterhoff I or II can be done by examining the average of their period distributions and comparing them to those in the MW GCs (see Table 2). Based on this criteria, the RR Lyraes in the stream field most resemble the OoI population. The average periods of the disk stars would lead us to believe that the disk may be slightly intermediate with average periods of RRab and RRc types being slightly higher than OoI, but lower than OoII. (We will see below, however, that this field more closely resembles OoI.) We note that the average period for c-types in the disk is higher, due to the presence of star 4302. Excluding this star, the average period for RRc stars in the disk is 0.320, in the range of the OoI type value. Likewise, we confirm the results of Paper I of the halo11 field being intermediate type. The numbers of stars in the halo21 and halo35b fields are too sparse to meaningfully interpret them, but seem to likely be OoI.

In Figure 12 we present Bailey diagrams for the RR Lyrae stars in these fields (including the halo11 field, plotting with the updated values as listed in Table 9), with the solid lines representing the relations for OoI and OoII classes of the Milky Way GCs (Clement 2000). For this plot, we converted the observed F606W amplitudes to V band amplitudes. To do this, we took the F606W and F814W photometry from the well-sampled, best fit light curve templates for each individual star (see Section 3.2), and applied a color-dependent transformation to convert the observed magnitudes to the standard V and I bandpasses. To perform this transformation, we used the synthetic stellar spectra of the MARCS model set (Gustafsson et al. 2008), an assumed extinction of $E(B -$

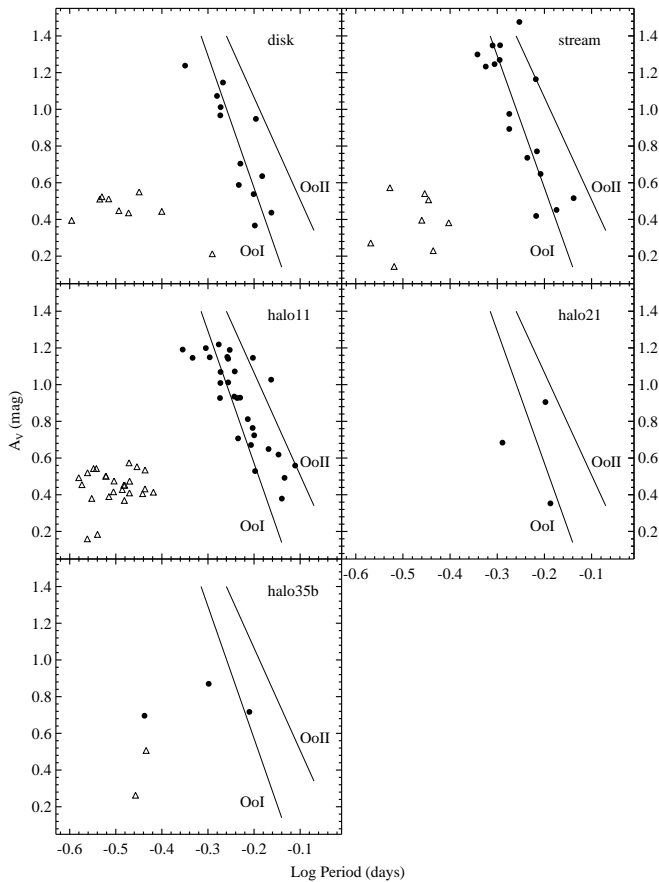


Figure 12. Bailey diagram for the RR Lyrae stars in our fields. The solid lines represent the Oosterhoff classes of the Milky Way globular clusters (Clement 2000). The circles are the ab-type stars and the triangles represent the c-type RR Lyraes. The halo11 field appears to be an intermediate case between Oosterhoff types. The stream appears to be of OoI type, as expected given the ratio of c-type and average period of ab-types. The disk also seems to prefer to OoI type, despite its ratio of c-type RR Lyrae to total RR Lyrae being closer to an intermediate type. Data of the halo21 and halo35b fields are too sparse to know for sure which Oosterhoff class the populations best resemble, although they appear to cluster towards the OoI locus.

$V) = 0.08$ (Schlegel et al. 1998), and the extinction curve of Fitzpatrick (1999). Once this transformation of the light curve in F606W to V was done, we determined the amplitude of the pulsations in V .

In this figure, we represent the ab-type stars with circles, and the c-type stars with open triangles. This diagram confirms the intermediate-type population of the halo11 field, and that the stream field RR Lyraes are likely OoI type. It also indicates the disk population is most likely OoI type, despite its ratio of c-type RR Lyrae to total RR Lyrae stars being intermediate of the two types, and its average RR ab period slightly higher than OoI type. It is unclear as to why there is this small difference, but despite it, we classify the disk as OoI. While the halo21 and halo35b appear to have a tendency toward the OoI type, we emphasize that the statistics in these fields are too limited to meaningfully interpret them.

4.3. RR Lyrae Reddenings

Guldenschuh et al. (2005) showed that the minimum-light color of an RR ab star can be used to estimate its line-of-sight reddening. For RR ab stars with periods between 0.39 and 0.7 days and metallicities ranging from $[Fe/H] \sim -3$ to 0, they find that intrinsic color depends very little on period or metallicity. They find that the color of these variables at minimum-light is $(V - I)_{0,min} = 0.58 \pm 0.02$.

Armed with this information, we are able to calculate the reddening of each of the RR ab stars in our fields. To do this, we use the V and I magnitudes, as calculated in Section 4.2. The observed $(V - I)$ color at minimum light was calculated from the best fit light curve template, and then used to calculate the reddening, $E(V - I)$, given the intrinsic value. We plot the distribution of these calculated reddenings in Figure 13. The vertical dashed line in this figure is the line of sight reddening for M31, $E(B - V) = 0.08$ (Schlegel et al. 1998), converted to $E(V - I)$ using the reddening relations of Cardelli, Clayton, & Mathis (1989). In this same figure, the average of each distribution is indicated by the vertical dotted line. This average, along with the standard deviation of the distribution is listed on each panel. This gives us an estimate of the error in the reddening of each field.

In addition to this error, we explored any error introduced by how well the template fitting program (see Section 3.2) could recover the minimum light color of the synthetic light curves described in Section 3.1. The mean difference between the synthetic minimum light color and the fit color was 0.008 magnitudes, less than the standard deviation of the reddening distributions in our fields, and adding little to the previously quoted error.

We note the peak of the distribution of the halo11 field is at the average value for Andromeda, confirming that there is likely little dust adding to the reddening in this part of the galaxy. The stream reddening is less than the average value. It is unclear to us as to why this is, but examination of the CMD (see Figure 3) indicates that the RR Lyraes in this field are, on average, bluer than those in the other fields.

Most of the disk stars fall at somewhat higher reddening than the average line-of-sight reddening for M31. This is not surprising given the higher amounts of gas and dust in the galactic disk. This higher-than-average reddening value may affect the age determined for the disk by the main sequence turn off (Brown et al. 2006, see especially their Table 6). The assumption of a larger reddening value would imply the intrinsic population is bluer and brighter, which would yield younger ages and lower metallicities than those determined by Brown et al. (2006) for the disk field.

5. METALLICITY AND DISTANCE

It has been found that the period and other pulsation properties of an RR Lyrae star can be used to determine its metallicity (e.g., Alcock et al. 2000; Sarajedini et al. 2006), and the star's absolute magnitude, and hence distance. Here we discuss various approaches for determining the metallicity of the ab-type stars (including the implied distance moduli). We also review a few of the shortcomings of some of the commonly used relations. After discussing and comparing these relations for the ab-type stars, we discuss the c-type stars.

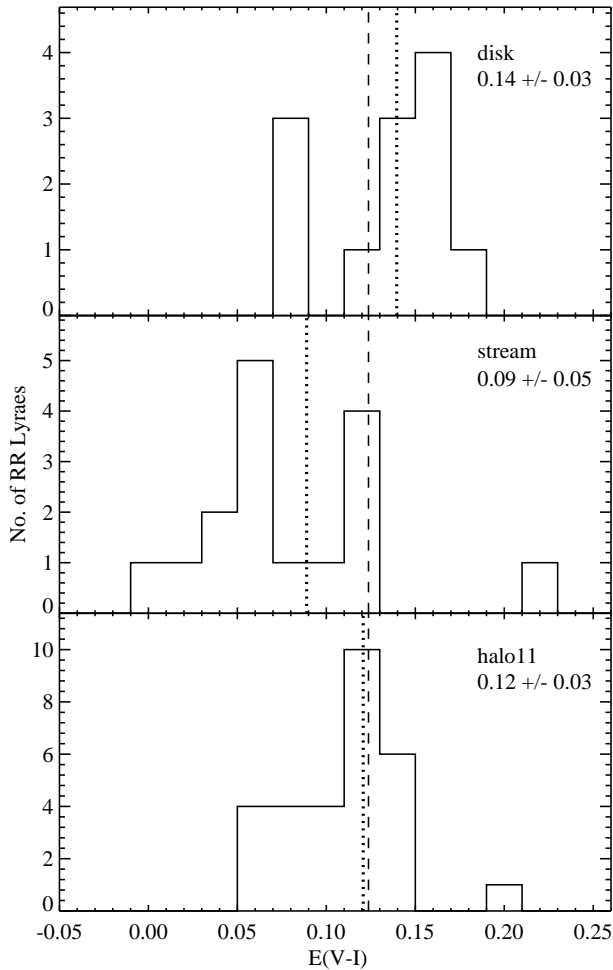


Figure 13. Distributions of $E(V-I)$ for RR_{ab} stars in the three fields of our sample with a significant RR Lyrae population. The vertical dashed line represents the average line-of-sight reddening for M31 (Schlegel et al. 1998), while the vertical dotted line is the average of each distribution. The average reddening and standard deviation are indicated on each panel.

5.1. The Period-Metallicity Relation

One simple relation for determining RR Lyrae metallicities was derived by Sarajedini et al. (2006, hereafter S06) by fitting data from A.C. Layden of 132 Galactic RR Lyrae stars in the solar neighborhood. The relation they found is

$$[Fe/H] = -3.43 - 7.82 \log P_{ab} \quad (1)$$

where P_{ab} is the period of the RR_{ab} stars in days. This relation is valid for metallicities between -2.5 and 0.0 . S06 used this relation to determine the metallicity distribution function (MDF) of the RR Lyrae stars they found in M33. As they note, this relation is similar in form to that determined by Sandage (1993). Errors for this relation are large (rms ~ 0.45 dex).

Using this relation, we present the normalized MDF for each of our M31 fields in the top row of panels of Figure 14. We calculate the average of each distribu-

tion and list these values in Table 15. Two errors are quoted for each field: the first is the standard deviation, the second (in parenthesis) is the standard error of the mean. They are calculated in the usual way, except for the halo21 and halo35b fields. In these cases we use the formulae appropriate for small statistical samples. The standard deviations agree with the expected accuracy of the technique (~ 0.45 dex).

For ab-stars with short periods, this relation can produce supersolar metallicities. We note that it is for this reason that we exclude star 7085 in the halo35b field throughout this analysis (see Section 4.1) as its short period would produce such an outlying metallicity. While such a value may be valid, S06 note that their metallicity relation was not derived for such high metallicities. While this star is still used when normalizing the sparse distribution of this field, we will disregard it in our subsequent analysis of this field, as it would highly skew any statistics, due to the already small sample of this field. In particular, we note that the average $[Fe/H]_{RRab}$ value for halo35b in Table 15 excludes this outlier, and we also exclude it in the distance calculation for this field.

It is important to understand the limitations of Equation 1 when determining $[Fe/H]$ values for individual RR_{ab} stars. First, as noted above, the rms dispersion in the $[Fe/H]$ values given by this equation is very large, and thus any individual determination will be quite uncertain. More importantly, Equation 1 is inconsistent with the fundamental pulsation equation, since it contains no information about the location of an RR_{ab} star within the instability strip. According to van Albada & Baker (1971) the pulsation period of an RR_{ab} star depends on the mass M , the luminosity L and the effective temperature T_{eff} as follows:

$$\log P_{ab} = 11.497 - 0.68 \log M + 0.84 \log L - 3.48 \log T_{eff} \quad (2)$$

where M and L are in solar units. Thus an RR_{ab} star located near the fundamental red edge of the instability strip would have a longer period and thus smaller $[Fe/H]$ value according to Equation 1 than an RR_{ab} star with the same mass and luminosity located near the fundamental blue edge. This is not a small effect. Consider, for example, the OoI cluster M3 for which there is no observational evidence for a significant variation in $[Fe/H]$. HB simulations show that the bulk of RR_{ab} stars in M3 have very similar masses and luminosities. Thus the variation in $\log P_{ab}$ across the instability strip in M3 comes primarily from the variation in T_{eff} . Canonical HB tracks show that the RR_{ab} stars in M3 are evolving blueward along blue loops as they cross the instability strip. Equation 1 would therefore imply that the $[Fe/H]$ values for such stars should increase during their evolution even when their masses and luminosities are constant. The size of this effect can be estimated from the pulsation periods obtained by Corwin & Carney (2001) in their study of the M3 RR Lyrae stars. Their data show that most RR_{ab} stars in M3 have periods between $\log P_{ab} = -0.15$ and -0.35 , implying a difference of 1.5 dex in $[Fe/H]$ between the reddest and bluest RR_{ab} stars in contradiction to the observed abundances. It is not surprising therefore that the $[Fe/H]$ values obtained from Equation 1 show such a large dispersion among the field RR_{ab} stars.

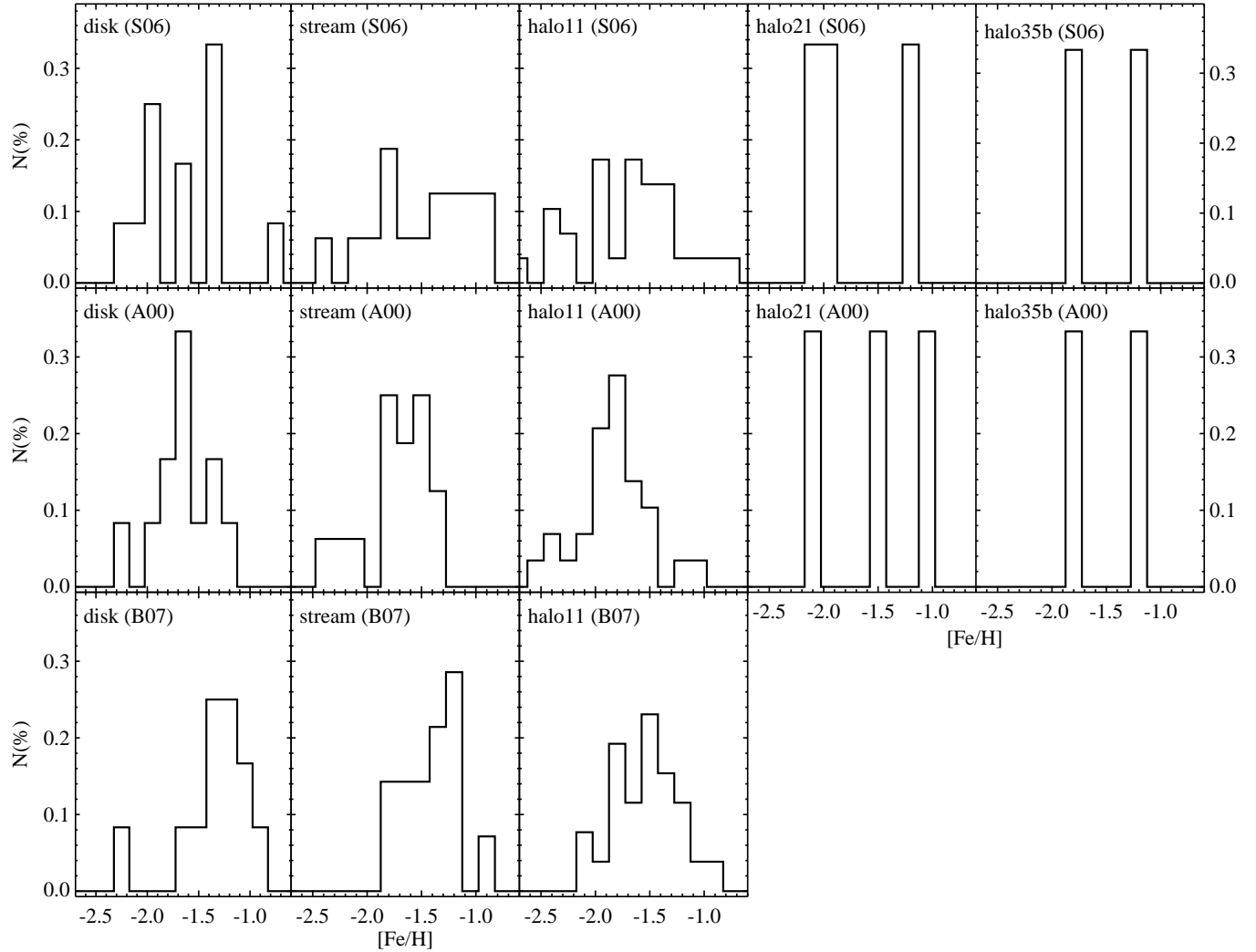


Figure 14. Normalized metallicity distributions for the ab-type RR Lyrae stars for each field calculated with the three different methods, as labeled. The panels are tiled in such a way for easy comparison of the MDFs produced by each method in each field. We have listed the average, standard deviation, and standard error of the mean of each of these distributions in Table 15. We note that the MDF of the halo35b field excludes star 7085, although it is used when normalizing the MDF. (See text for discussion).

[Fe/H]	disk	stream	halo11	halo21	halo35b
S06	$-1.58 \pm 0.42(0.12)$	$-1.44 \pm 0.45(0.11)$	$-1.63 \pm 0.46(0.09)$	$-1.67 \pm 0.47(0.27)$	$-1.44 \pm 0.61(0.43)$
A00	$-1.57 \pm 0.26(0.08)$	$-1.65 \pm 0.31(0.08)$	$-1.77 \pm 0.33(0.06)$	$-1.53 \pm 0.64(0.37)$	$-1.40 \pm 0.51(0.36)$
B07	$-1.29 \pm 0.36(0.10)$	$-1.32 \pm 0.29(0.07)$	$-1.47 \pm 0.30(0.06)$	–	–
RR _c	-1.70	-1.65	-1.43	–	-1.88

Table 15

Summary of the average calculated metallicities of the RR Lyrae in our M31 fields. The method used is indicated in the first column. Errors quoted are the standard deviations of the respective distribution, with the standard error of the mean in parenthesis. For the A00 and S06 methods, the standard deviation of the metallicity for the disk, stream, and halo11 fields are consistent with the expected accuracy of the method ($\sigma_{[Fe/H]} \sim 0.31$ and 0.45 , respectively). No errors are given for metallicities using the c-type variables, as no error estimates were estimated or provided for the relation in the original source.

We do however recognize that this relation is usually only meant to be used when the amplitudes of RR Lyraes are very uncertain or unavailable. When this relation is the only viable option, however, it is important that authors proceed with great caution, given these great uncertainties.

When calculating the distance modulus, $(m - M)_0$, for each field, we must first determine the average apparent magnitude of each star in the V band. The transformation of the F606W to the V band was done as we described in Section 4.2.

Carretta et al. (2000) derive a relationship between an RR Lyrae star's metallicity and its absolute magnitude. Once we know the metallicities of the RR Lyrae stars, we can determine its absolute magnitude using their relation:

$$M_V = (0.18 \pm 0.09) * ([Fe/H] + 1.5) + (0.57 \pm 0.07). \quad (3)$$

We use this relation and the average metallicity determinations for the RR_{ab} stars to calculate the average absolute magnitude of the RR Lyraes in each field. We then subtract it from the average unreddened V magnitude of each respective field to determine the unreddened distance modulus. For the disk, stream, and halo11 fields the reddenings used were those calculated as outlined in Section 4.3. Reddening for the halo21 and halo35b was assumed to be $E(B - V) = 0.08 \pm 0.03$ because of the low number of RR Lyrae in these two fields. (This is a valid assumption, given the low amounts of dust in the halo.) We list the result of this in Table 16.

The error of the absolute magnitude for each star is calculated by propagating the errors of Equation 3, and assuming an error on metallicity (standard deviation) for each field as listed in Table 15. Errors in the average unreddened apparent magnitude for each field are calculated as the standard error of the mean of the sample. The final quoted errors of Table 16 are done by adding in quadrature the errors on apparent magnitude, absolute magnitude, and (for the halo21 and halo35b) absorption.

Our results are in agreement within the error bars with previous distance determinations of M31 using RR Lyraes. For example, Sarajedini et al. (2009) find a distance of $(m - M)_0 = 24.46 \pm 0.11$. (We note that our errors are larger because we propagated our metallicity error to the end.) Our results also agree with the Cepheid distance to M31, $(m - M)_0 = 24.44 \pm 0.1$ (Freedman & Madore 1990).

5.2. The Period-Amplitude-Metallicity Relation

Among the most frequently used relations to determine the metallicity of RR_{ab} stars was found by Alcock et al. (2000, hereafter A00). They found a period-amplitude-metallicity relation for ab-type stars in the form

$$[Fe/H]_{RR_{ab}} = -8.85[\log P_{ab} + 0.15A(V)] - 2.60, \quad (4)$$

where $A(V)$ is the amplitude in the V band and P_{ab} is the period in days. This relation has been used in many previous studies, including Paper I and Sarajedini et al. (2009), and is similar to the relation found by Sandage

(2004). When applying this relation to our data, we calculated the V band amplitude as described in Section 4.2.

We plot the normalized MDF for each field in the middle row of panels in Figure 14. The average of the MDF for each field is given in Table 15. Again, two errors are quoted for each field, the standard deviation and the standard error of the mean (in parenthesis). And as before, these values for the halo21 and halo35b fields use the formulae appropriate for small statistical samples.

A00 note that the accuracy of this technique is $\sigma_{[Fe/H]} \sim 0.31$. Standard deviations of the MDF for the disk, stream, and halo11 fields (i.e., the fields with a substantial enough RR Lyrae population to produce a well-populated MDF) are consistent with the accuracy of the technique.

Sarajedini et al. (2009) use the A00 relation to determine the metallicities of a sample of RR Lyrae stars in the spheroid of M31 and compare the resulting MDF to the MDF found using the S06 relation (Equation 1). They find the results to be similar. We also find these two distributions to be similar when applied to our sample. The average metallicity values from the A00 method agree within the error bars to the S06 metallicities. As before, we excluded star 7085 in the halo35b field from the analysis (see Section 5.1).

At first glance the A00 relation for the RR_{ab} metallicity would appear to be an improvement over the S06 relation, because it includes a term involving the amplitude $A(V)$ which provides a measure of a star's location within the instability strip. Unfortunately, this is not the case. As emphasized by Bono et al. (2007), the form of any period-amplitude-metallicity relation depends strongly on the choice of calibrating clusters (see their Figure 5). The A00 relation was calibrated on the clusters M15, M3 and M5. However, the use of other clusters can yield a quite different calibration and hence quite different values of $[Fe/H]$. Essentially the A00 relation is an attempt to determine the metallicity from the size of the period shift in the Bailey diagram of the RR_{ab} stars. However, Figure 5 of Bono et al. (2007) shows, for example, that the period shift is negligible among the OoI globular clusters over a wide range in $[Fe/H]$ from -1.8 to -1.1.

Once metallicities are found, we calculate absolute magnitudes and distance moduli for each field, using the same method as described in the previous section. Results are listed in Table 16.

5.3. The Bono Method

The relations we have discussed thus far have been frequently used by RR Lyrae researchers in numerous studies, and are therefore useful for putting our results into a similar context for comparison. However, the physical reliability of these relations has been recently questioned by a number of studies in the literature.

A recent paper by Catelan (2009) shows that there is no clear trend in the mean RR_{ab} period with metallicity for the OoI clusters, contrary to what the A00 and S06 relations indicate (i.e., that an increase in period leads to a decrease in metallicity, at constant $A(V)$). The errors of derived $[Fe/H]$ values from both the A00 and S06 relations are high, which lead to high errors in distance when properly propagated through the relations

$(m - M)_0$	disk	stream	halo11	halo21	halo35b
S06	24.50 ± 0.22 (794)	24.56 ± 0.22 (817)	24.49 ± 0.23 (791)	24.37 ± 0.29 (748)	24.35 ± 0.24 (741)
A00	24.50 ± 0.22 (794)	24.60 ± 0.23 (831)	24.51 ± 0.23 (798)	24.34 ± 0.29 (738)	24.35 ± 0.23 (741)
B07(1.5)	24.34 ± 0.12 (738)	24.47 ± 0.20 (783)	24.40 ± 0.08 (759)	–	–
B07(2.0)	24.51 ± 0.12 (798)	24.62 ± 0.18 (839)	24.55 ± 0.07 (813)	–	–
RR _c	24.61 ± 0.12 (836)	24.43 ± 0.12 (769)	24.47 ± 0.12 (783)	–	24.41 ± 0.17 (762)
Weighted Average	24.49 ± 0.17 (791)	24.52 ± 0.19 (802)	24.48 ± 0.15 (787)	24.36 ± 0.40 (745)	24.38 ± 0.27 (752)

Table 16

Summary of the calculated distances of the RR Lyraes in our M31 fields. The method used is indicated in the first column. The B07(1.5) and B07(2.0) methods indicate the results using $\alpha = 1.5$ and 2.0, respectively. Errors of the distance calculated from the c-type stars (last row) are much smaller than the other methods because they do not include error in metallicity. The numbers in the parenthesis below each distance modulus value is that distance modulus value converted to Mpc.

between metallicity and absolute magnitude. (Often RR Lyrae researchers drop the absolute error bars on metallicity when calculating errors of absolute magnitude, and hence distance modulus, reporting distance errors that are much smaller than one would expect, given the large error in metallicity.)

Bono et al. (2007, hereafter B07) addressed some of the uncertainties in the RR Lyrae relationships by deriving equations relating the observed quantities of these pulsators (e.g., RR*ab* period and $A(V)$) to actual physical properties of the star (e.g., luminosity and mass). They did this using nonlinear hydrodynamical models for the RR*ab* pulsation. These equations depend modestly on the assumed mixing length ratio α in the models, so they considered two values, $\alpha = 1.5$ and 2.0. Their analysis yielded relations between M_V and the RR*ab* periods and $A(V)$. Given the values of the M_V , one can then derive the metallicity by adopting an appropriate metallicity- M_V relation. This method is therefore the reverse of the methods discussed above: rather than first calculating metallicities and then absolute magnitudes (and hence distances), this technique first calculates the absolute magnitude and then the metallicity.

In their study, B07 define a parameter k_{puls} for both values of α as

$$k(1.5)_{puls} = 0.136 - \log P_{ab} - 0.189A(V) \quad (5)$$

$$k(2.0)_{puls} = 0.027 - \log P_{ab} - 0.142A(V) \quad (6)$$

Additionally, they find that the average absolute magnitude, $\langle M_V \rangle$, of a population's RR Lyraes stars is related to the average of the k_{puls} parameter ($\langle k_{puls} \rangle$), in the following relations (their Equations 5 and 6), again, listed for both mixing length values:

$$\langle M_V^{k(1.5)} \rangle = 0.12(\pm 0.10) + 2.65(\pm 0.07) \langle k(1.5)_{puls} \rangle \quad (7)$$

$$\langle M_V^{k(2.0)} \rangle = 0.14(\pm 0.10) + 2.67(\pm 0.07) \langle k(2.0)_{puls} \rangle \quad (8)$$

For metallicities greater than -1.0 , they give the following relations (their Equations 8 and 9):

$$M_V^{k(1.5)} = 0.56 - 0.49A(V) - 2.60 \log P_{ab} + 0.05[Fe/H] \quad (9)$$

$$M_V^{k(1.5)} = 0.64 - 0.49A(V) - 2.60 \log P_{ab} + 0.20[Fe/H] \quad (10)$$

for $-1.0 \leq [Fe/H] \leq -0.5$ and $-0.5 \leq [Fe/H] \leq 0.0$, respectively.

The above Equations 7 and 8 can be used to find the distance modulus of the metal poor stars (i.e., $[Fe/H] \leq -1.0$, where the relations are valid) in the population of interest. B07 did this for the globular cluster ω Cen, for both possible values of the mixing length. They plotted the unreddened visual magnitudes of the cluster RR*ab* stars against the k_{puls} parameter for each star (see their Figure 17). These data are then fit with a straight line with the slope of the above Equations 7 and 8. The difference between this line and the line defined by these equations, i.e., the shift in magnitude needed to match the data, is the distance modulus. The distance values found by B07 for ω Cen using the different α values bracket the accepted distance value, indicating that the proper value for α is likely near 1.7. Unfortunately, however, no equations were provided for this best value.

We have done this same analysis for the ab-type stars in our disk, stream, and halo11 fields, where the population sample is big enough to get meaningful results.⁸ In Figure 15 we have plotted the unreddened magnitude values for the RR*ab* stars (using the individual reddening values found in Section 4.3) and then calculated the corresponding k_{puls} values. The panels on the left are for $\alpha=1.5$, while those on the right are for $\alpha=2.0$. The solid line is a best fit (using a standard linear least squares fitting technique) of a straight line with the slope of Equations 7 and 8 (on the respective plots). The best fit distance modulus in each case is listed in Table 16, for both values of α . The accompanying error is the error of the fit. Similar to the B07 results, our results likely bracket the true value which probably lies within the error bars of both.

⁸ As we will show in Section 5.4, it is possible to apply this method to individual stars; however, deriving a distance modulus from the method of fitting a straight line to V_0 vs. k_{puls} plot, requires a large enough sample, as we have here.

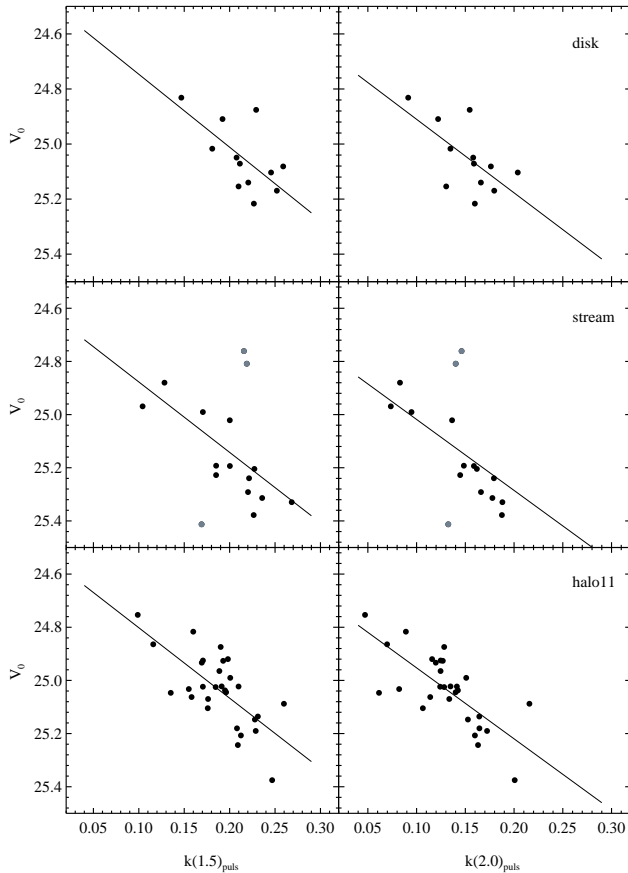


Figure 15. Unreddened visual magnitude V_0 of RR_{ab} in the disk, stream, and halo11 fields, plotted versus $k(1.5)_{puls}$ (left panels) and $k(2.0)_{puls}$ (right panels). The solid lines are Equations 6 and 7 (in the respective panels) and account for the intrinsic distance modulus. The distance modulus found from the best fit is listed in Table 16. See text for discussion.

Because this method of finding the distance is independent of a calculated metallicity, we note that the errors are lower than the previous two methods (although they all agree within the errors). Not only that, it relies on a method that is much more physical, and therefore likely more reliable. We note the extreme outlying points in the stream field (the gray points) leading to higher distance errors in this field compared to the disk or halo11 field. The two high outlying points are stars 561 and 2933, while the low outlying point is star 2577. The fits of the light curves of 561 and 2933 (see Figure 7) are poorer than for the other stars, possibly explaining why these stars are outliers. Despite this, we retain these stars in our analysis.

In addition to the distance calculations, B07 derive a relation between metallicity and absolute magnitude, valid over the metallicity range of $[Fe/H] = -2.5$ to ~ 0 . The relation is

$$M_V^{k(1.5)} = 1.19(\pm 0.10) + 0.50[Fe/H] + 0.09[Fe/H]^2. \quad (11)$$

Using this relation, we calculated individual $[Fe/H]$ values from the values of $M_V^{k(1.5)}$ given by Equation 7 for

the RR Lyrae stars in each of these three fields. The MDF constructed in this manner is shown as the bottom row of panels in Figure 14. We have listed the average, standard deviation, and standard error of the mean of these MDFs in Table 15, as before.

We note that errors on metallicity for our fields using the B07 method are mostly comparable to those of the A00 and S06 methods. However, one major advantage of the B07 method is that these metallicity errors do not propagate into distance errors as they do with the other methods.

Our results for distance using the method of B07 are consistent within the errors with those found in the previous section, which is encouraging. The metallicity values are overall slightly more metal rich (compare values in Table 15). However, because the B07 results were derived using a more physically meaningful, consistent way, we believe they are a better representation of the actual physical values of this sample of RR Lyraes. Relative metallicities remain nearly the same when compared to the other two methods.

B07 also found that the distribution of the k_{puls} parameter can potentially be a useful indicator of the Oosterhoff type. They determined that the location of the peak in the distribution of k_{puls} is dependent on its Oosterhoff type. Also, they note that the distribution of OoII clusters is slightly different for clusters that have a horizontal branch (HB) bluer than $+0.8^9$ when compared to those whose HBs do not extend that far.

We plot these distributions in Figure 16. The top three panels of this plot are taken from B07 (see their Figure 8), and show the distribution of $k(1.5)_{puls}$ for OoI and OoII clusters, as labeled. The bottom three panels are these distributions for our disk, stream, and halo11 fields. As can be seen from this plot, the stream and the disk are indeed more similar to the OoI type (given the peak and shape of their distributions) while the halo11 field is an intermediate population. We note however, that it is possible that the halo11 field is a mixed population, with some combination of OoI and OoII. This scenario would be consistent with the findings of Sarajedini et al. (2009) who find fields in the halo of M31 at 4 and 6 kpc to be OoI.

5.4. Comparison with the Layden Data

In order to test the previous three methods, we have compared the metallicities given by these methods with those determined spectroscopically for 78 field ab-type RR Lyrae stars from an unpublished dataset from A.C. Layden (private communication). This will allow us to use the measured periods and amplitudes to determine how well the different methods reproduce the actual metallicities of these stars.

We display the results of this in Figure 17. The top plot is the difference in metallicity calculated by each method minus Layden's spectroscopic value as a function of Layden's metallicities, with the color and symbols as indicated. (We remind the reader that the B07 metallicities are calculated using only $\alpha = 1.5$, as they do not provide a metallicity relation for $\alpha = 2.0$. Additionally,

⁹ This parameter is defined as $(B - R)/(B + V + R)$ between the numbers of HB stars to the blue (B), within (V), and to the red (R) of the RR Lyrae instability strip (Lee 1990).

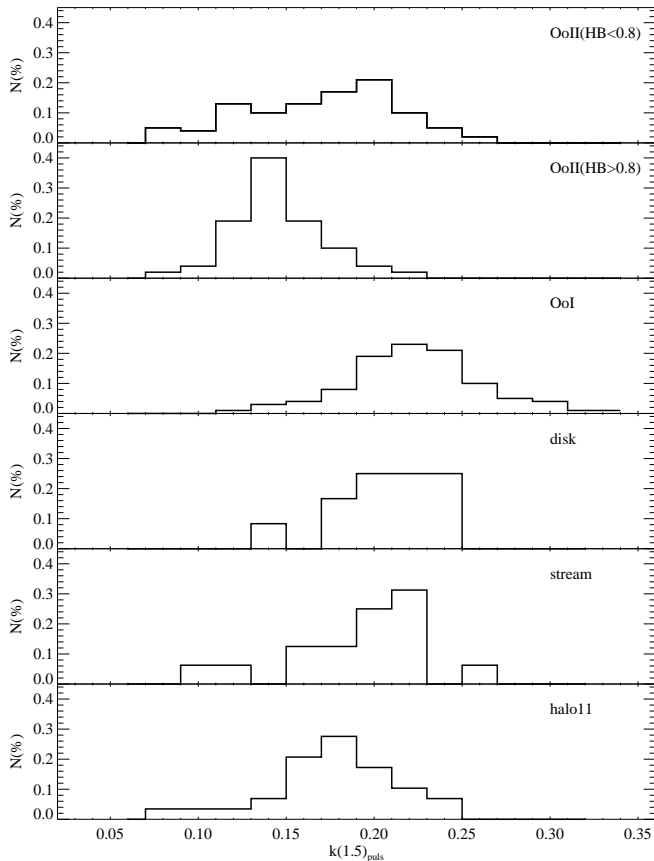


Figure 16. The distribution of the $k(1.5)_{puls}$ parameter for MW GCs of different Oosterhoff type (as labeled), as well as for the disk, stream, and halo11 fields. As is evident from this plot, we confirm that the stream and the disk are likely OoI type, while the halo11 field is an intermediate population, or possibly a mixed population of OoI and OoII.

we note that we used the proper M_V relation, given the metallicity of each star, see Equations 7, 9, and 10, when solving for the metallicity, Equation 11.) The horizontal solid line is at a difference equal to 0.

The three panels in the bottom plot of this same figure are histograms of the above differences, giving us an idea of how well each method reproduces the spectroscopic values. Again, the solid vertical line is at difference of 0. We have fit a Gaussian distribution to each histogram and overplot it to help quantify the method’s ability to reproduce the metallicities and the error. The numbers on the plot indicate the average and standard deviation of the Gaussian.

The average difference of each of the three methods comes out to nearly zero, which is encouraging. The S06 (period-metallicity) method does the poorest job of the three at reproducing the spectroscopic metallicity values, and it has the largest spread ($\sigma \sim 0.5$). However, this isn’t surprising because it has the least information going into the calculation (i.e., it uses periods alone, not amplitudes). The A00 (period-amplitude-metallicity) method does a better job with a tighter distribution, although it is systematically off by nearly 0.25 dex. This is likely because of the choice of calibrating GCs in determining the zero point and slope in the relation (see Equation 4).

The errors we find on these two methods are consistent with the expected uncertainty for an individual star (~ 0.31 and 0.45 for A00 and S06, respectively.)

The B07 method does the best job of reproducing the spectroscopic metallicities, closely centered around zero difference, although the A00 and S04 methods both agree within the errors. The spread in these distributions is roughly consistent with what we see in our M31 data (see Table 15). However, because metallicity errors of the B07 method do not propagate through to the absolute magnitude (and hence distance) calculations, and the derivation is more physical, B07 is our preferred method.

5.5. The c-type Stars

The RRc stars also exhibit a relation between period and metallicity. However, unlike the ab-type stars, this relation relies on the average period of the c-type variables in a given population, rather than individual stellar properties. This is calculated using the relation (from Sandage 1993)

$$[Fe/H]_{RRc} = (-\log \langle P_c \rangle - 0.670)/0.119 \quad (12)$$

where $\langle P_c \rangle$ is the average period of the c-type RR Lyrae stars. Because this method calculates metallicity from the mean properties of a population, a single number for each field is determined, rather than a distribution like the ab-type stars. We note the value calculated by this method in Table 15. We also note that we have not quoted errors for the metallicity calculated from the RRc stars, as no error estimates were provided for the above equation. Given this metallicity, we then calculated the distance to each field using Equation 3, in the same manner as before. These values are listed in Table 16.

Regardless of the method used, we desire to compare the metallicities calculated here with those calculated by detailed studies of the CMDs of these fields (Brown et al. 2006), as well as spectroscopic work (e.g., Guhathakurta et al. 2006). These studies found the populations to be, on average, more metal rich than calculated here by about 0.5 to 1.0 dex. The reason for this is that the RR Lyrae stars pre-select towards the metal poor tail of the respective population distributions. However, we note that the relative metallicities (at least those calculated by methods that use the RRab stars) are similar: e.g., the disk is more metal rich than the halo and the stream, and the stream is more metal rich than the halo.

6. SUMMARY AND CONCLUSIONS

We have presented a complete survey of the RR Lyrae stars in six ultra deep fields in various parts of M31: namely, the disk, the giant stellar stream, and halo fields of varying distance from the galactic center. We find RR Lyraes in five of the six fields. The halo11 field is of intermediate (or mixed) Oosterhoff type, the disk and the stream are of OoI type; the halo21 and halo35b fields seem to have a tendency toward OoI type, but are too sparse to meaningfully classify as one type or the other. We determine the average reddening of the disk, stream, and halo11 fields and find that the disk is more reddened

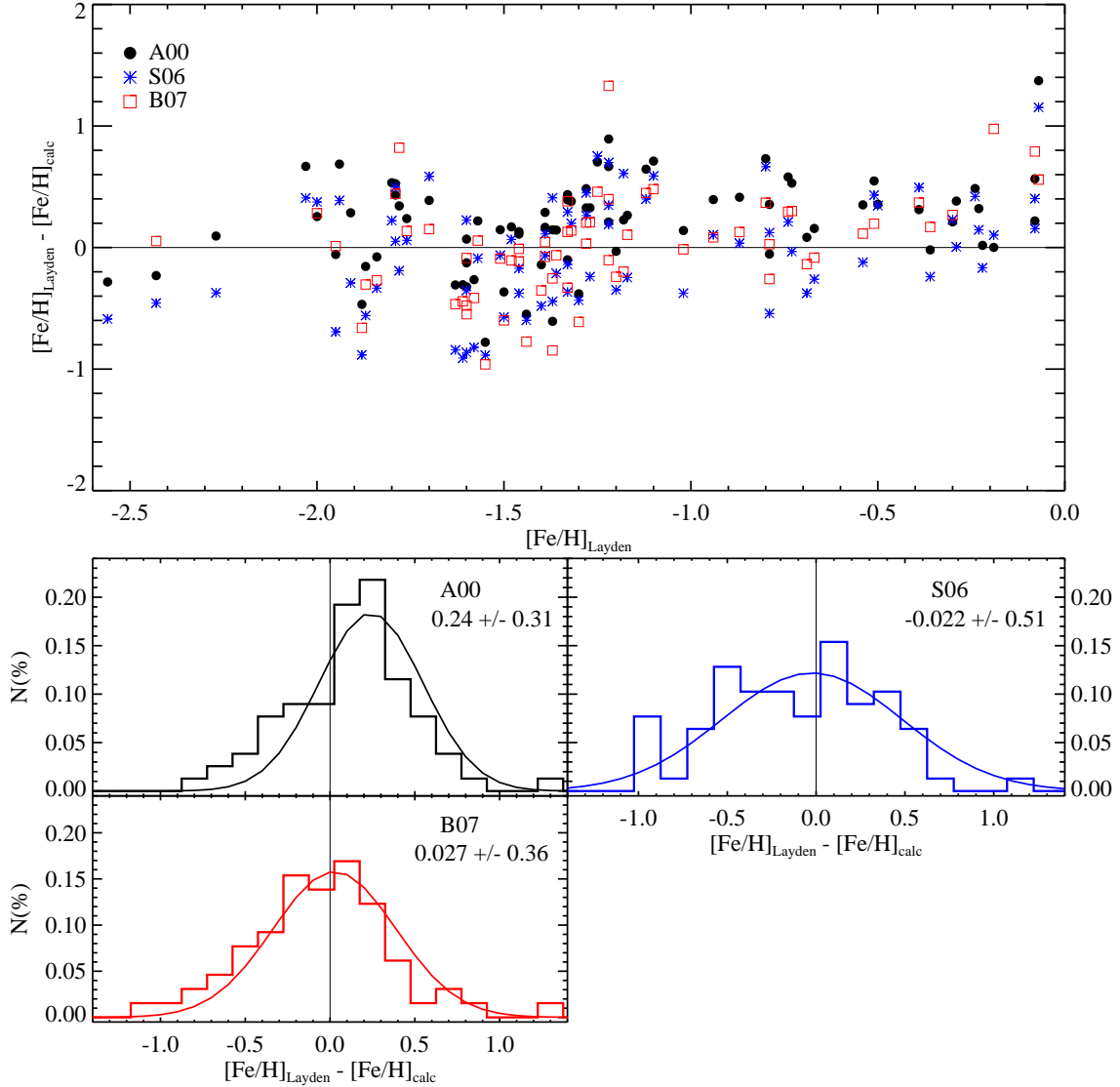


Figure 17. A comparison of the three methods we have used for calculating RR Lyrae metallicities. The top plot is the difference in the metallicity calculated minus the spectroscopic value vs. the spectroscopic metallicity, with the colors and symbols as indicated. The horizontal solid line is at a difference equal to 0. The panels in the bottom plot are histograms of the above differences, with a best fit Gaussian to each distribution overplotted. The numbers on the plot indicate the average and standard deviation of the Gaussian, and aid in quantifying how well each method can reproduce the “true” metallicity.

than the literature value to M31, while the halo11 is roughly the same.

We have calculated metallicities and distances for each field of our sample, using a variety of methods including the period-metallicity relation of Sarajedini et al. (2006), the period-amplitude-metallicity of Alcock et al. (2000), and the method of Bono et al. (2007) that is derived from more physically realistic models (using two values for the mixing length), rather than simple empirical relations. These three methods are roughly consistent, although the latter method has smaller errors than the former on distance though errors are similar for metallicity.

To compare these three methods for calculating metallicities, we have applied each of these methods to data of MW field RR Lyraes. We found that although the three methods tend to overlap and be consistent within the errors, the B07 method is our preferred method. It not

only provides closest match and is based on more physical derivations, but importantly, high metallicity errors do not propagate through to distance calculations, as with the more traditional methods.

Acknowledgments

We wish to thank A.C. Layden for kindly providing us with his data for the field RR Lyrae stars. We would also like to thank Ata Sarajedini for helpful discussions in the later stages of this paper. We acknowledge support for Programs GO-9453, GO-10265, and GO-10816 was provided by NASA through a grant from the Space Telescope Science Institute, which is operated by the Association of Universities for Research in Astronomy, Incorporated, under NASA contract NAS5-26555. We are also grateful for the useful comments of an anonymous

referee, which helped to clarify this paper.

REFERENCES

- Alcock, C. et al. 2000, *AJ*, 119, 2194 (A00)
- Alonso-Garcia, J., Mateo, M., & Worthey, G. 2004, *AJ*, 127, 868
- Bedin, L.R., Piotto, G., Anderson, J., Cassisi, S., King, I.R., Momany, Y., & Carraro, G. 2004, *ApJ*, 605, L125
- Bono, G., Caputo, F. & Di Criscienzo, M. 2007, *A&A*, 476, 779 (B07)
- Blazhko, S. 1907, *Astron. Nachr.*, 175, 325
- Brown, T.M., Ferguson, H.C., Smith, E., Kimble, R.A., Sweigart, A.V., Renzini, A., Rich, R. M., VandenBerg, D.A. 2003 *ApJ*, 592, L17
- Brown, T.M., Ferguson, H.C., Smith, E., Kimble, R.A., Sweigart, A.V., Renzini, A., Rich, R.M. 2004, *AJ*, 127, 2738 (Paper I)
- Brown, T.M., Smith, E., Ferguson, H.C., Rich, R.M., Guhathakurta, P., Renzini, A., Sweigart, A.V., Kimble, R.A. 2006, *ApJ*, 652, 323
- Brown, T.M., Smith, E., Ferguson, H.C., Guhathakurta, P., Kalirai, J.S., Rich, R.M., Renzini, A., Sweigart, A.V., Reitzel, D., Gilbert, K.M., Geha, M. 2007, *ApJ*, 658, L95
- Brown, T.M., Beaton, R., Chiba, M., Ferguson, H.C., Gilbert, K.M., Guhathakurta, P., Iye, M., Kalirai, J.S., Koch, A., Komiyama, Y., Majewski, S.R., Reitzel, D.B., Renzini, A., Rich, R.M., Smith, E., Sweigart, A.V., Tanaka, M. 2008, *ApJ*, 685, L121
- Brown, T.M., Smith, E., Ferguson, H.C., Guhathakurta, P., Kalirai, J.S., Kimble, R.A., Renzini, A., Rich, R.M., Sweigart, A.V., Vanden Berg, D.A. 2009, *ApJS*, 184, 152
- Cacciari, C., & Renzini, A. 1976, *A&AS*, 25, 303
- Carretta, E., Gratton, R.G., Clementini, H., & Fusi, P.F. 2000, *ApJ*, 533, 215
- Catelan, M. 2004, *ASPC*, 310, 113
- Catelan, M. 2009, *Astrophysics Space Sci*, 320, 261
- Catelan, M., Grundahl, F., Sweigart, A.V., Valcarce, A.A.R., Corts, C. 2009, *ApJ*, 695, L97
- Cardelli, J.A., Clayton, G.C., & Mathis, J.S. 1989, *ApJ*, 345, 245
- Chaboyer, B. 1999, in *Post Hipparcos Cosmic Candles*, ed. A. Heck & F. Caputo (Dordrecht: Kluwer), 111
- Chiaberge, M., Lim, P.L., Kozhurnia-Platais, V., Sirianni, M., & Mack, J. 2009, *ACS Instrument Science Report* 09-01
- Clement, C.M. 2000, in *IAU Colloq. 176, The Impact of Large-Scale Surveys on Pulsating Star Research*, ed. L. Szabados & D.W. Kurtz (ASP Conf. Ser. 203) (San Francisco: ASP), 266
- Clement, C.M., Muzzin, A., Dufton, Q., Ponnampalam, T., Wang, J., Burford, J., Richardson, A., Rosebery, T., Rowe, J., Hogg, H.S. 2001, *AJ*, 122, 2587
- Clementini, G., Federici, L., Corsi, C., Cacciari, C. Bellazzini, M., & Smith, H.A. 2001, *ApJ* 559, L109
- Contreras, R., et al. 2008, *Mem. Soc. Astron. Ital.*, 79, 686
- Contreras, R., Catelan, D., Smith, H.A., Pritzl, B.J., & Borissova, J. 2005, *ApJ*, 623, L117
- Corwin, T. M., & Carney, B. W. 2001, *AJ*, 122, 3183
- Dolphin, A.E., Saha, A., Olzsewski, E., Thim, F., Skillman, E.D., Gallgher, J.J., & Hossel, J. 2004, *AJ*, 127, 875
- Ferguson, A.M.N., Irwin, M.J., Ibata, R.A., Lewis, G.F., Tanvir, N.R. 2002, *AJ*, 124, 1452
- Fiorentino, G., Monachesi, A., Trager, S., Lauer, T., Saha, A., Mighell, K., Freedman, W. L., Dressler, A., Grillmair, C. J., Tolstoy, E. 2010, *ApJ*, 708, 817
- Fitzpatrick, E.L. 1999, *PASP*, 111, 63
- Freedman, W.L. & Madore, B.F. 1990, *ApJ*, 365, 186
- Guhathakurta, P., et al. 2006 *AJ*, 131, 2497
- Guldenschuh, K.A., et al. 2005, *PASP*, 117, 721
- Gustafsson, B., Edvardsson, B., Eriksson, K., Jorgensen, U.G., Nordlund, A., Plez, B. 2008, *A&A* 486, 951
- Layden, A.C. 1995, *AJ*, 110, 2312
- Layden, A.C., & Sarajedini, A. 2000, *AJ*, 119, 1760
- Lomb, N.R. 1976, *Ap&SS*, 39, 447
- Makidon, R. B., Lallo, M. D., Casertano, S., Gilliland, R. L., Sirianni, M., Krist, J. E., 2006 *SPIE Proceedings* Vol. 6270
- Oosterhoff, P. Th. 1939, *Observatory*, 62, 104
- Piotto, G., King, I.R., Djorgovski, S.G., Sosin, C., Zoccali, M., Saviane, I., De Angeli, F., Riello, M., Recio-Blanco, A., Rich, R. M., Meylan, G., Renzini, A. 2002, *A&A*, 391, 945
- Piotto, G., Villanova, S., Bedin, L.R., Gratton, R., Cassisi, S., Momany, Y., Recio-Blanco, A., Lucatello, S., Anderson, J., King, I.R., Pietrinferni, A., Carraro, G. 2005, *ApJ*, 621, 777
- Pritchett, C.H. & van den Bergh, S. 1987, *ApJ*, 316, 517
- Pritzl, B.J., Smith, H.A., Catelan, M., & Sweigart, A.V. 2000, *ApJ*, 530, L41
- Pritzl, B.J., Armandroff, T.E., Jacoby, G.H., & Da Costa, G.S. 2002, *AJ*, 124, 1464
- Rich, R.M., Sosin, C., Djorgovski, S.G., Piotto, G., King, I.R., Renzini, A., Phinney, E.S., Dorman, B., Liebert, J., Meylan, G. 1997, *ApJ*, 484, L25
- Reiss, A. & Mack, J. 2004, *ACS Instrument Science Report* 04-06
- Sandage, A. 1993, *AJ*, 106, 687
- Sandage, A. 2004, *AJ*, 128, 858
- Sarajedini, A., Barker, M., Geisler, D., Harding, P., & Schommer, R. 2006, *AJ*, 132, 1361 (S06)
- Sarajedini, A., Mancone, C.L., Lauer, T.R., Dressler, A., Freedman, W., Trager, S.C., Grillmair, C., & Mighell, K.J. 2009, *AJ*, 138, 184
- Scargle, J.D. 1982, *ApJ*, 263, 835
- Schlegel, D.J., Finkbeiner, D.P., & Davis, M. 1998, *ApJ*, 500, 525
- Siegel, M.H., & Majewski, S.R. 2000, *AJ*, 120, 284
- Suntzeff, N.B., Kinman, T.D., & Kraft, R.B. 1991, *ApJ*, 367, 528
- van Albada, T. S., & Baker, N. 1971, *ApJ*, 169, 311
- Yoon, S.-J., Seok-Joo, J., Ree, C.H., Han, S.-I., Kim, D.-G., & Young-Wook, L. 2008, *ApJ*, 677, 1080
- Zinn, R. & Searle, L. 1976, *ApJ*, 209, 734